ECAP-2018

Sensitivity studies with intrinsic limit neutrino resolution for KM3NeT/ORCA

Bachelorarbeit aus der Physik

Vorgelegt von
Sebastian Konrad
14.08.2018

Erlangen Centre for Astroparticle Physics
Physikalisches Institut IV
Friedrich-Alexander-Universität Erlangen-Nürnberg

1. Gutachter: Dr. Thomas Eberl
2. Gutachter: Prof. Dr. Gisela Anton

Abstract

The determination of the neutrino mass hierarchy might be possible due to matter effects. Oscillstion experiments like water and ice Cherenkov detectors are build to measure the neutrino oscillation probability in Earth. But to get certainty on the results the dectors have to be sensitive for certain neutrino energy regimes.
This thesis deals with the sensitivity of the KM3NeT/ORCA detector for the neutrino mass hierarchy by using simulations (paramNMH). For a better understanding of the detector and for possible improvements in reconstructing events different assumptions were made. The instrinsic limits were taken to get the best possible resolution and to determine what the detector is optimally capable of measuring. Additionally the reconstructed mean energy was altered for the $\bar{\nu}$ compared to ν in order to account for different light yields. The particle identification capability was further variated to see its impact on sensitivity.

Contents

1 Neutrino oscillations and neutrino mass hierarchy

In the 1960s a discrepancy between the predicted neutrino flux (ν_e) from the sun and the measured flux was observed. In the Davis experiment only one third of the expected neutrinos were measured. This led to the discussion whether the experiment or the theory had flaws. The resolution of this solar neutrino puzzle was proposed by Pontecorvo (1968). He argued that if neutrinos had mass they would be able to change their flavour. That would explain why less neutrinos of the solar flux were detected, because some of the neutrinos had changed their flavour. The first prove of oscillation was given by Takaaki Kajita with the Super-Kamiokande experiment with atmospheric neutrinos (see section 3) in 1998. The detector consists of 50 kilotons clear water and 11,146 photomultiplier [16] and measured the neutrino composition for atmospheric neutrinos to determine if the predicted flux for each flavour matched the hypothesis of flavour oscillations. T. Kajita was rewarded with a nobel price for his work in this field (2015).
After that the Sudbury Neutrino Observatory (SNO) did a similar experiment for solar neutrinos to finally solve the solar neutrino problem [3].
One implication of the Super-Kamiokande experiment was that not all neutrinos can have zero mass. The flavour eigenstates $\nu_\alpha(\alpha = e, \mu, \tau)$ are linear combinations of the mass eigenstates $\nu_i(i = 1, 2, 3)$. The transformation from flavour eigenstates to mass eigenstates is given by:

$$\begin{pmatrix}\nu_e\\ \nu_\mu\\ \nu_\tau\end{pmatrix} = \underbrace{\begin{pmatrix}1 & 0 & 0\\ 0 & c_{23} & s_{23}\\ 0 & -s_{23} & c_{23}\end{pmatrix}\begin{pmatrix}c_{13} & 0 & s_{12}e^{-i\delta}\\ 0 & 1 & 0\\ -s_{13}e^{-i\delta} & 0 & c_{13}\end{pmatrix}\begin{pmatrix}c_{12} & s_{12} & 0\\ -s_{12} & c_{12} & 0\\ 0 & 0 & 1\end{pmatrix}}_{\mathcal{U}_{PMNS}}\begin{pmatrix}\nu_1\\ \nu_2\\ \nu_3\end{pmatrix} \quad (1)$$

where $c_{ij} = \cos\theta_{ij}$ and $s_{ij} = \sin\theta_{ij}$ and $\mathcal{U}_{PMNS}$ is the Pontecorvo-Maki-Nakagawa-Sakata neutrino mixing matrix.
The ORCA experiment (and oscillation experiments in general) is not sensitive to the absolut neutrino masses, only to the squared-mass splittings ($\Delta m^2_{ij} = m^2_i - m^2_j$ with $i, j = 1, 2, 3$). For further understanding of the neutrino and its attributes (e.g CP-violating phase δ, Majorana/Dirac particle) the ordering of the neutrino masses or their squared-mass splittings is important. Due to atmospheric and solar measurements two squared-mass difference are known [1],[6, 453]. Due to matter effect in the sun the determination of the sign of the mass splitting between the first and the second mass eigenstate Δm^2_{21} is possible (see Equation 2). This allows two possibilites for the neutrino mass hierarchy: normal hierarchy (NH) $m_1 < m_2 < m_3$ and inverted hierarchy (IH) $m_3 < m_1 < m_2$.
(see Figure 1.1)

$$\Delta m^2_{SOL} = \Delta m^2_{21} \ll \Delta m^2_{ATM} = |\Delta m^2_{31}| \quad (2)$$

It is also known that:

$$\Delta m^2_{21} \ll \Delta m^2_{31} \simeq \Delta m^2_{32}. \quad (3)$$

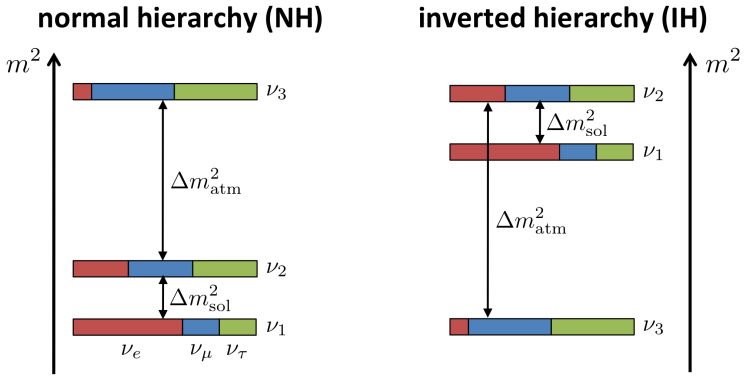

Figure 1.1: Normal and inverted hierarchy as possible ways of neutrino mass ordering [9]

The mass eigenstates $|\nu_i\rangle$ for a neutrino that is emitted of time $t = 0$ and location $x = 0$ develop like [19, 194]:

$$|\nu_i(x,0)\rangle = e^{ipx} |\nu_i\rangle . \tag{4}$$

For a relativistic particle [19, 194]

$$E_i = \sqrt{m_i^2 + p_i^2} \simeq p_i + \frac{m_i^2}{2p_i} \simeq E + \frac{m_i^2}{2E} \tag{5}$$

is valid. With

$$|\nu_\alpha\rangle = \sum_i U_{\alpha i} |\nu_i\rangle \qquad \text{and} \qquad |\nu_i\rangle = \sum_\alpha U^*_{\alpha i} |\nu_\alpha\rangle \tag{6}$$

the oscillation probability for CP invariance (U_α is real) is given by [19, 195]

$$P(\alpha \to \beta)(t) = \delta_{\alpha\beta} - 4 \sum_{j>i} U_{\alpha i} U_{\alpha j} U_{\beta i} U_{\beta j} \sin^2 \left(\frac{\Delta m^2_{ij}}{2} \frac{L}{E} \right) . \tag{7}$$

Where L is the length from source to detector. This gives the probabilities [19, 119]

$$\begin{aligned} P(\nu_\mu \to \nu_\tau) &= \sin^2(2\theta_{23}) \cos^4(\theta_{13}) \sin^2 \left(\frac{\Delta m^2_{13} L}{4E} \right) , \\ P(\nu_e \to \nu_\mu) &= \sin^2(2\theta_{13}) \sin^2(\theta_{23}) \sin^2 \left(\frac{\Delta m^2_{13} L}{4E} \right) , \\ P(\nu_e \to \nu_\tau) &= \sin^2(2\theta_{13}) \cos^2(\theta_{23}) \sin^2 \left(\frac{\Delta m^2_{13} L}{4E} \right) . \end{aligned} \tag{8}$$

2 Neutrino oscillations in matter

If neutrinos do propagate in matter, matter effects occur and modify the oscillation probability. ν_e and $\bar{\nu_e}$ can interact via neutral current (NC) and charged current (CC) interactions (see Figure 2.1) [19, 220].

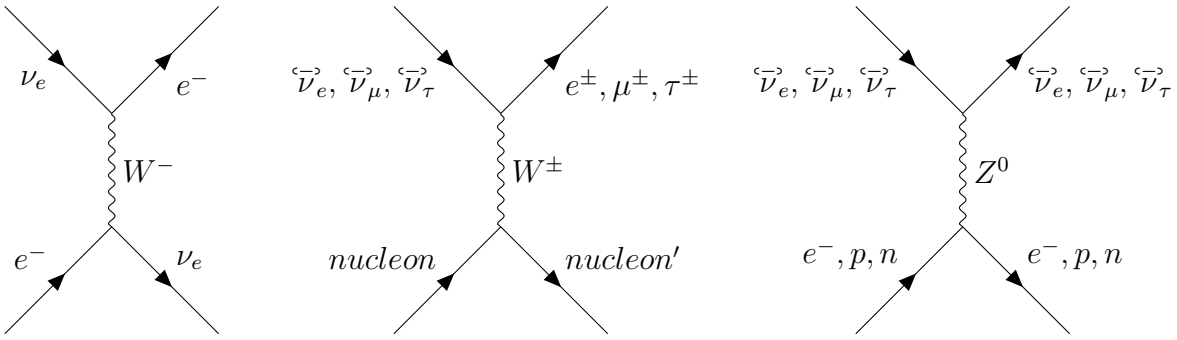

Figure 2.1: Coherent weak foward scattering on electron for CC (left), CC event at nucleon (middle) and NC event with Z^0 at different particles (right)

The probability of a NC interaction is equal for each flavour [19, 220]. But because there are normally no μ or τ but e^- and nucleons in matter, there is an additional interaction possible for ν_e via CC (Figure 2.1). This changes the oscillation probability by adding an additional term $\mathcal{H}_1$ to the vacuum Hamiltonian in the flavour basis,

$$\mathcal{H}_1 = A \begin{pmatrix} 1 & 0 & 0 \\ 0 & 0 & 0 \\ 0 & 0 & 0 \end{pmatrix} = \pm\sqrt{2} G_F N_e \begin{pmatrix} 1 & 0 & 0 \\ 0 & 0 & 0 \\ 0 & 0 & 0 \end{pmatrix}, \tag{9}$$

where G_F is the Fermi weak coupling constant and N_e the electron density [15]. The sign is dependent whether it is a neutrino (+) or an antineutrino (-). This leads to the total Hamiltonian [12]

$$\mathcal{H}_{tot} = \mathcal{H}_0 + \mathcal{H}_1 = \mathcal{U}\mathcal{H}_0\mathcal{U}^{-1} + \mathcal{H}_1, \tag{10}$$

which is not diagonal neither in the mass nor the flavour eigenstate basis.
This leads to a shifted squared mass difference in matter. In the for simplicity reduced two neutrino mixing problem, the mass difference between the first and the third mass eigenstate in vacuum changes into an effective mass difference Δm^2_{13eff}.

$$\Delta m^2_{13eff} = \Delta m^2_{13} \sqrt{(\cos(2\theta_{13}) - A_{eff})^2 + \sin^2(2\theta_{13})}, \tag{11}$$

with

$$A = \pm \frac{2\sqrt{2} G_F N_e E_\nu}{\Delta m^2_{13}}. \tag{12}$$

The mixing angle θ_{13} is also converted to into an effective mixing angle:

$$\tan(2\theta_{13}^{eff}) = \frac{\tan(2\theta_{13})}{1 - \frac{A_{eff}}{\cos(2\theta_{13})}}. \tag{13}$$

For

$$A = \cos(2\theta_{13}), \tag{14}$$

the effective mixing angle becomes maximal and the effective mass becomes minimal. That leads to a maximal mixing. This resonant mixing was first proposed by Mikheyev, Smirnov and Wolfenstein [17]. The so called MSW-effect is obtained for a neutrino with an energy [14]:

$$E_{\nu}^{res} = \pm \frac{\Delta m_{13}^2 \cos(2\theta_{13})}{2\sqrt{2} G_F N_e}. \tag{15}$$

The matter effects allow a conclusion whether the NH or the IH is realised in nature. That is possible due to Equation 11 and Equation 12. In the NH, Δm_{13}^2 has a positive sign and in the IH a negative sign and for the resonance to take place A must be positive in Equation 11. That means for neutrinos (positive sign) in Equation 12 Δm_{13}^2 must be greater than zero (NH) and for antineutrinos (negative sign) the IH must be true to obtain the resonance.
To sum this up: For the NH we see the resonance for neutrinos and for IH we see the resonance for antineutrinos. This gives the opportunity to determine which neutrino mass hierarchy is realised in nature.

3 Atmospheric neutrinos

There are two kinds of neutrino experiments: the ones with an artificial source (reactor, collider) and the ones where naturally occuring neutrinos are used. Possible sources for the last kind are the sun, radioactive materials, cosmic neutrinos or atmospheric neutrinos.
The atmospheric neutrinos are the ones that are exploited in KM3NeT/ORCA. Atmospheric neutrinos are created when cosmic radiation interacts with Earth's atmosphere.

3.1 Atmospheric neutrino flux

The cosmic flux consists mostly of protons and heavier ionised nuclei. Those are deflected by interstellar and intergalactic magnetic fields and come to Earth in isotropic manner. By interaction with the atmosphere pions (see also Figure 3.1) and kaons are created. Those pions and kaons decay and produce atmospheric neutrinos:

$$\begin{aligned} \pi^- &\longrightarrow \mu^- \bar{\nu}_\mu \longrightarrow e^- \bar{\nu}_e \nu_\mu \bar{\nu}_\mu, \\ \pi^+ &\longrightarrow \mu^+ \nu_\mu \longrightarrow e^+ \nu_e \bar{\nu}_\mu \nu_\mu, \end{aligned} \tag{16}$$

$$\begin{aligned} K^- &\longrightarrow \pi^- \pi^0 \longrightarrow 2\gamma + \mu^- \bar{\nu}_\mu \longrightarrow 2\gamma + e^- \bar{\nu}_e \nu_\mu \bar{\nu}_\mu, \\ K^+ &\longrightarrow \pi^- \pi^0 \longrightarrow 2\gamma + \mu^+ \nu_\mu \longrightarrow e^+ \nu_e \bar{\nu}_\mu \nu_\mu. \end{aligned} \tag{17}$$

For every ν_e and $\bar{\nu}_e$, two $\nu_\mu/\bar{\nu}_\mu$ are created which leads to:

$$(\nu_\mu + \bar{\nu}_\mu)/(\nu_e + \bar{\nu}_e) \approx 2. \tag{18}$$

Because the flux of cosmic rays is isotropically distributed we would expect an isotropic atmospheric neutrino flux. But that is not the case, because the neutrino flux is higher at the horizon. That is caused by the higher probability of μ to decay, because they propagate longer in thinner medium which lowers the integrated interaction probability in comparison to μ from the zenith. So normally the flux from above should be the same for each flavour like the flux from below. But the neutrinos from below have to pass Earth and are influenced by neutrino oscillation in matter.

3.2 Matter effects in Earth with atmospheric neutrinos

Atmospheric neutrinos traversing Earth is a possible solution to sort out the mass ordering due to the matter resonance like discussed in section 2. To determine where the resonance is located (in the energy spectrum, see Figure 3.4), Earth's density profile (electron density) and the energy of the neutrino must be known. Earth's density depends on the radius (see Figure 3.2), because the core is denser than the mantle. That means the electron density of the core is higher than of the mantle which leads to an alternated oscillation probability.

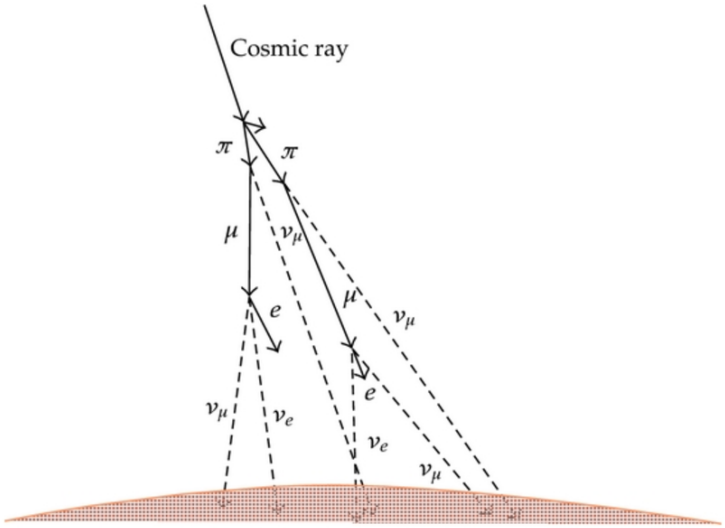

Figure 3.1: Schematic production of atmospheric neutrinos[10]

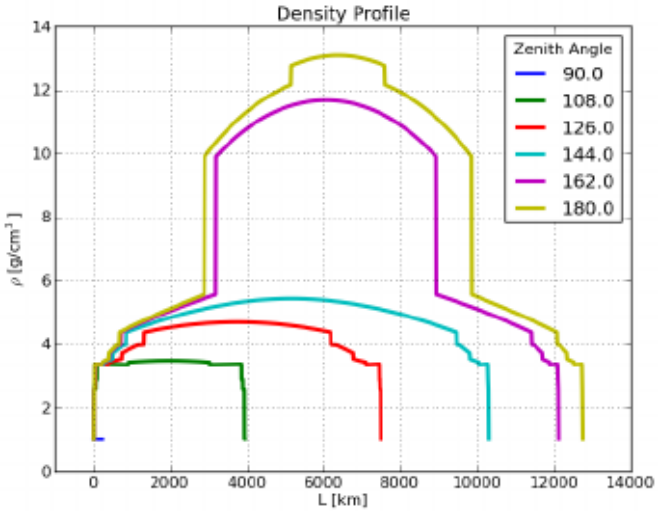

Figure 3.2: Density profile of Earth for different zenith angles [13]

As it is shown in Figure 3.4 the resonance is seen for neutrinos in the NH and for antineutrinos in the IH. The matter effects are seen for about 3 GeV to 10 GeV. For the model the energy dependency of the neutrino flux has to be considered (see Figure 3.3). This plot is very dependent on which different atmospheric neutrino flux model (HKKM15, Bartol, Fluka) is used. That leads to an uncertainty in the modulation.

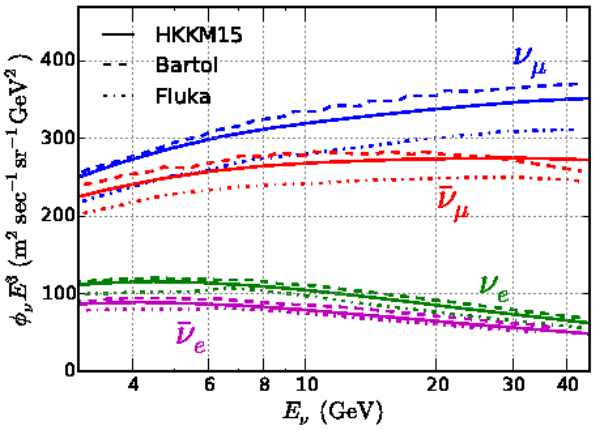

Figure 3.3: Energy dependency of the atmospheric neutrino flux [18]

Also the zenith angle dependency is seen in the oscillogramm (Figure 3.4) and the different oscillation probabilities whether the neutrino traverses Earth's core or mantle.

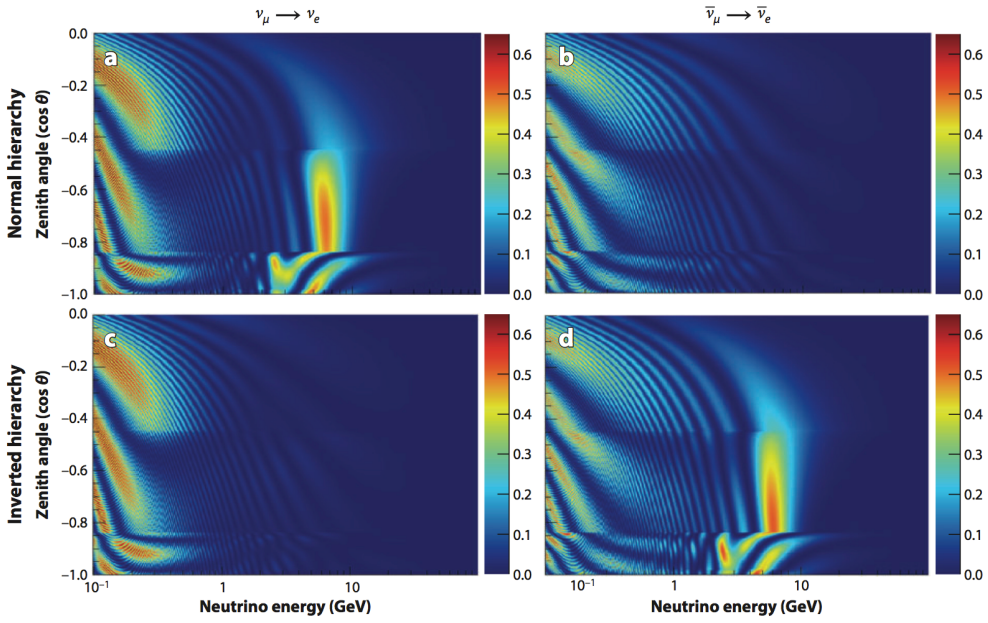

Figure 3.4: Neutrino oscillation probability for different neutrino energies and zenith angles with a) NH $\nu_\mu \longrightarrow \nu_e$ b) NH $\bar{\nu}_\mu \longrightarrow \bar{\nu}_e$
c) IH $\nu_\mu \longrightarrow \nu_e$ d) IH $\bar{\nu}_\mu \longrightarrow \bar{\nu}_e$ [11]

4 KM3NeT/ORCA

To detect the oscillation resonance in Earth (sec. 3.2) a huge detector is needed. The reason why, is that a great amount of events has to be detected in order to get a good certainty on the measurement. A 1 Mton detector expects about 4650 ν_μ-induced and 2850 ν_e-induced events per year (for energies over $4GeV$) [1]. The number of events scale with the detector size. The detector has to have an energy range in which the resonance occurs (3 GeV-10 GeV) and also a good understanding of the systematic effects and background.

4.1 Neutrino detection with KM3NeT/ORCA

When a neutrino interacts inside of the detector with a nucleus in an event described by Figure 2.1 charged particles are created. These ultrarelativistic particles produce Cherenkov light in water. This light is emitted in the so-called Cherenkov cone, which has a specific opening angle of 42°. The flavour of the incoming neutrino can be approximated by the light signal which is generated by the secondary particles of the CC reactions. For NC events the flavour cannot be determined, because the secondary shower is not flavour dependent. In principle the event topologies are distinguished between track-like and shower-like events. The appearance of a track like event indicates an incoming ν_μ CC event, because the produced μ has a longer mean free path than e or a τ.
The distinction between neutrinos and antineutrinos is done on a statistical basis. This is possible because ν and $\bar{\nu}$ have different interaction cross sections at the relevant energies [5]:

$$\sigma(\nu N) \approx 2 \cdot \sigma(\bar{\nu} N). \tag{19}$$

4.2 Construction of KM3NeT/ORCA

The signals of Cherenkov light, that are emitted through ultrarealtivistic particles, are measured with Digital Optical Modules (DOMs) in the KM3NeT/ORCA detector. Each DOM contains 31 photomultiplier tubes (PMTs). The ORCA detector consists of 115 strings with 18 DOMs per string (see Figure 4.1) with 9m vertical distance between the DOMs. The strings are 20m appart from each other (see Figure 4.2). This gives a whole detector volume of $\sim$ 5.7 Mt instrumented water and 64,000 PMTs

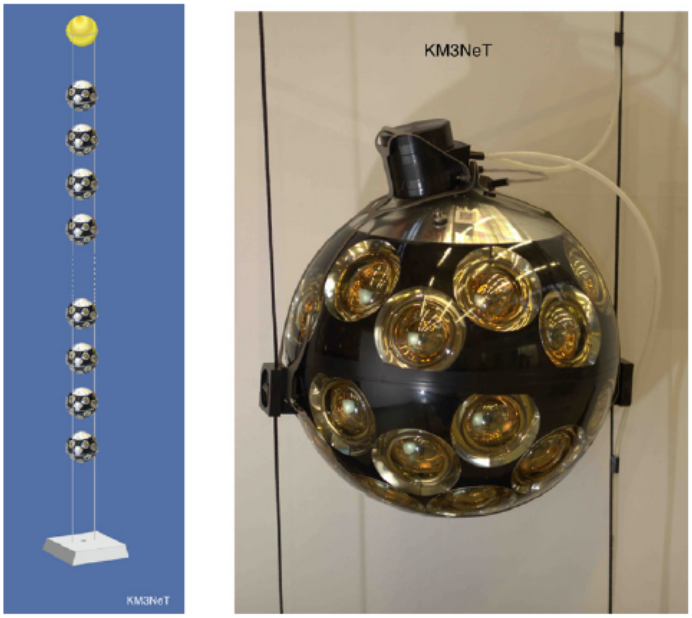

Figure 4.1: String (left) and Digital Optical Module [1]

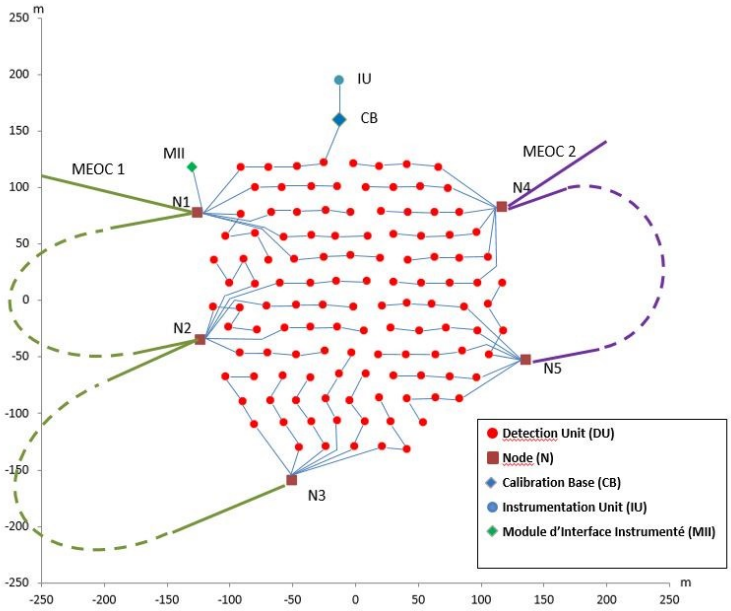

Figure 4.2: Planned KM3NeT/ORCA layout [4]

5 Sensitivity studies

To determine the neutrino mass hierarchy a good energy and angular resolution is needed. It is necessary to know which trajectory the neutrino had (angular resolution) to determine which density profile of Earth the neutrino has passed. This has influence on the oscillation (see section 3.2). The energy resolution is important for finding the energy dependent matter effects and reduce energy-smearing. There are mainly two possible effects on the resolution of the detector. One is the so-called intrinsic limit (see section 5.1). Those are the limits that are imposed by intrinsic physical fluctuations on the neutrino energy and the arrival direction reconstruction. The other effect is the reconstruction of an event.
To test the capability of the detector to verify the right neutrino mass hierarchy with the intrinsic limits the improvements have to be simulated. The examined improvements are the intrinsic limits for energy resolution (see section 5.2) and direction (see section 5.3), the effects of the light yield ratio on the mean energy (see section 5.4), the replacement of the $\overset{(-)}{\nu}_\mu$ energy resolution and mean energy (see section 5.5) and the Particle Identification (PID) (see section 5.6).
For sensitivity studies a program called paramNMH (version: d270c680 from April 30,2018) was used. paramNMH uses the parameterization for detector response and physical characteristics (e.g. neutrino flux) from the Letter of Intent for KM3NeT 2.0 [1], as input for the physics and detector response needed for a calculation of the sensitivity. In the first step neutrino flux information and interaction probabilities are used to get expected event rates in the detector as function of the true E_ν and θ_{zenith}:

$$R_a(E,\theta) = \frac{\rho_{water}}{m_{nucleon}} \cdot \sum_b \sigma_a(E) \cdot P^{osc}_{a,b}(E,\theta) \cdot \Phi^{atm}_b(E,\theta)[1] \tag{20}$$

with

- R_a the interaction rate per unit volume at the detector site of (anti)neutrinos of a flavour a as a function of E_ν and zenith angle θ
- initial flavour b is summed over $\nu_e, \nu_\mu, \bar{\nu}_e, \bar{\nu}_\mu$
- Φ^{atm}_b is the atmospheric neutrino flux for neutrinos of flavour b
- $P^{osc}_{a,b}$ is the oscillation probability for a neutrino passing through Earth
- σ_a is the CC neutrino-nucleon cross section for a neutrino of a flavour.

The atmospheric neutrino fluxes are taken from by the HKKM2014 model [8]. After that the response of the detector is modelled. That leads to the reconstructed events as a function of E_{reco} and θ^{reco}_{zenith}. For paramNMH a simplified approach was used with starting point of two histograms (for track and shower) in the reconstructed quantities E_{reco}, θ_{reco}. In each bin i is the expected number of events (μ^{TH}_i) for a given true hierarchy (TH) hypothesis is calculated. After that a χ^2-minimisation assuming the wrong hierarchy (WH) with the parameters from Table 5.1 is performed.

Parameter	True value	Treatment
θ_{23} [°]	{40,42,...,50}	variated
θ_{13} [°]	8.42	fixed
θ_{12} [°]	34	fixed
ΔM^2 $[10^{-3}eV^2]$	2.4	fitted
Δm^2 $[10^{-5}eV^2]$	7.6	fixed
δ_{CP} [°]	0	fitted
Overall flux factor	1	fitted
NC scaling	1	fitted
$\nu/\bar{\nu}$ skew	0	fitted
μ/e skew	0	fitted
Energy slope	0	fitted

Table 5.1: Parameters for the χ^2-minimisation of the wrong hierachy [1]

As result

$$\chi^2_{min} = \sum_i \frac{(\mu_i^{TH} - \mu_i^{WH_{fit}})^2}{\mu_i^{Th}} \qquad [1] \qquad (21)$$

is obtained. That leads to the statistical sensitivity

$$\sigma = \sqrt{\chi^2} \qquad [1] \qquad (22)$$

with which the WH can be excluded. paramNMH with its default parameters (from the Letter of Intent) was used as reference point for comparison.

5.1 Intrinsic limit on neutrino energy and angular resolution

The intrinsic limits can be determined by reconstructing the energy of the neutrino E_ν and the normalized direction $\vec{u}_\nu$. That is possible by combining the reconstructed lepton properties with that of the hadronic cascade:

$$\begin{aligned} E_\nu^{reco} &= E_l^{reco} + E_h^{reco}, \\ \vec{u}_\nu^{reco} &= \omega_l \frac{E_l^{reco}}{E_\nu^{reco}} \vec{u}_l^{reco} + \omega_h \frac{E_h^{reco}}{E_\nu^{reco}} \vec{u}_h^{reco}. \end{aligned} \qquad [2] \qquad (23)$$

The weights ω_l and ω_h are set to unity for naive four-momentum conservation approach. Because the intrinsic limits for muon tracks and electromagnetic cascades are signifcant smaller than those for the hadronic cascade, the neutrino resolution strongly depends on the inelasticity

$$y = \frac{E_h}{E_\nu} = \frac{E_\nu - E_l}{E_\nu}. \qquad [2] \qquad (24)$$

Figure 5.1 and Figure 5.2 show the neutrino energy resolution and angular resolution as functions of the neutrino energy. These plots are obtained if it is

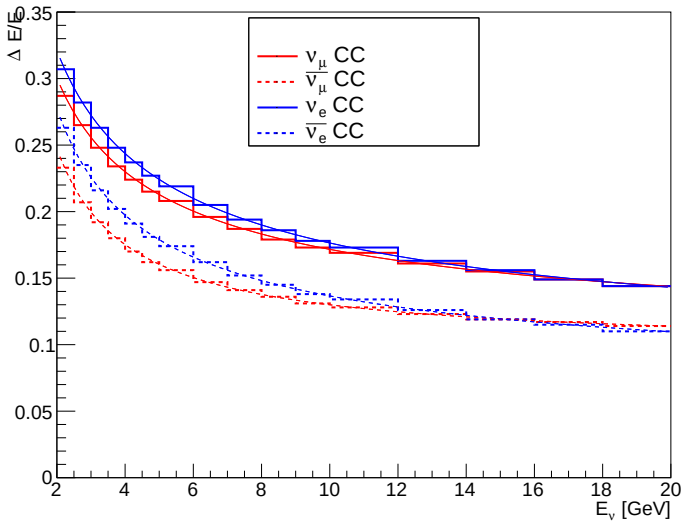

Figure 5.1: Parameterisation of the intrinsic limit for energy resolution, for ν_e (blue line), $\bar{\nu}_e$ (blue dots), ν_μ (red line) and $\bar{\nu}_\mu$ (red dots).

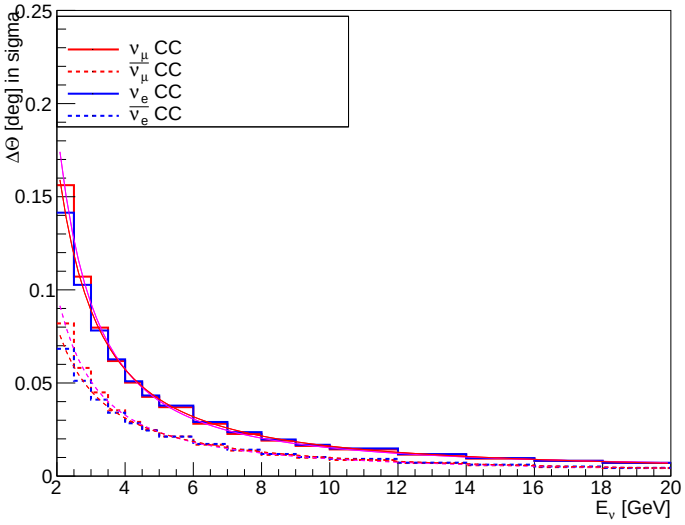

Figure 5.2: Parametrisation for intrisic limit for angular resolution for ν_e (blue line), $\bar{\nu}_e$ (blue dots), ν_μ (red line) and $\bar{\nu}_\mu$ (red dots).

intergrated over the corresponding y distributions.
For the next part the intrinsic limits for energy resolution (see Figure 5.1) and angular resolution (see Figure 5.2) [2] are parameterized[1]. Another effect that has influence on the sensitivity is the particle identification (PID). That means the probability that a track-like event is classified as such and the probability that a shower-like event is classified as a track-like event. It should also show which channel, track or shower, is more important to sensitivity and on which channel the modifications have more effect.
To be able to compare these adjustments the simulation for the normal reconstruction without adjustments is needed (paramNMH with default parameters). Figure 5.3 and Figure 5.4 show for which true energy which energy is reconstructed. It can be seen that the likelihood for reconstructing a certain energy to a certain true energy is given and it is similar to a straight line with a few exceptions[2]. The energy reconstruction is also more precise for $\overset{(-)}{\nu}_e$ (see Figure 5.3) than for $\overset{(-)}{\nu}_\mu$ (see Figure 5.4). Is has to be mentioned that the plots for ν and $\bar{\nu}$ are very similar to each other.

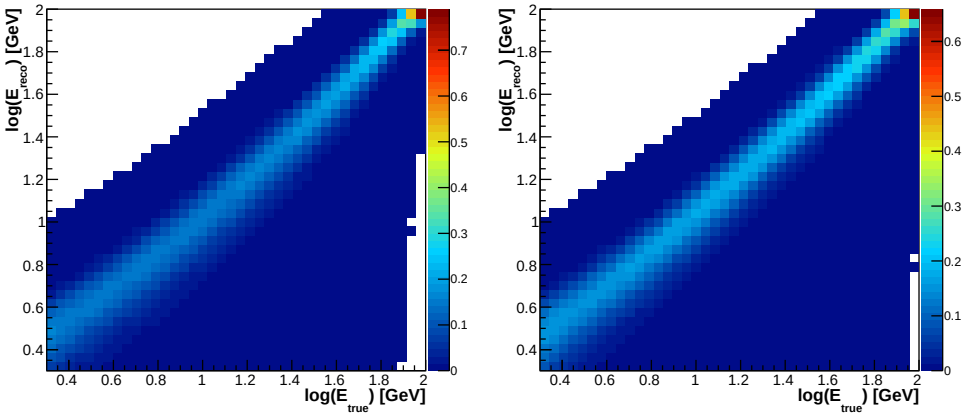

Figure 5.3: E_{reco} over E_{true} ν_e CC (left) and $\bar{\nu}_e$ CC (right) with no modifications. This resolution plot was done with paramNMH with default values. The colour code shows how high the probability is to reconstruct a certain energy. The reconstructed energy is Gaussian distributed.

Additional to the energy resolution a plot for the angular resolution was made (see Figure 5.5). This resolution plot was done with paramNMH with default values
On the left side of the figure the reconstructed angle is plotted over the true angle. The plot is taken for a fixed angle of $\cos(\theta_{true}) = 0.87$. Here the reconstruction gets better for higher energies. That is due to the fact that with a longer shower or track structure the angle is easier to determine. The plot on right (Figure 5.5) describes for which angles the detector and the reconstruction is sensitive. The plot is taken for a fixed energy $E = 8.26GeV$. The resolution seems to get better for angles near zero (vertical up-going), because the description is given for the $\cos(\theta)$ and not for θ.

[1] details in sections 5.2 and 5.3
[2] The 'straight' is slightly curved and the energy is also slightly overestimated

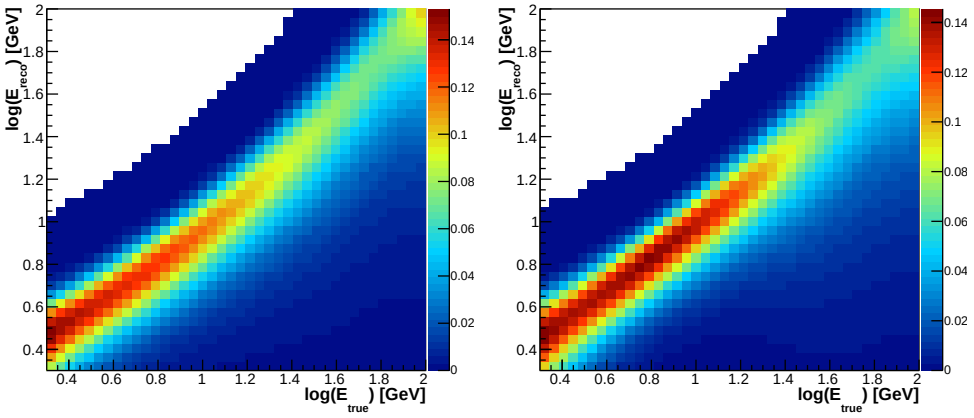

Figure 5.4: E_{reco} over E_{true} ν_μ (left) and $\bar{\nu}_\mu$ (right) with no modifications. This resolution plot was done with paramNMH with default values. The colour code shows how high the probability is to reconstruct a certain energy. The energy is Gaussian distributed.

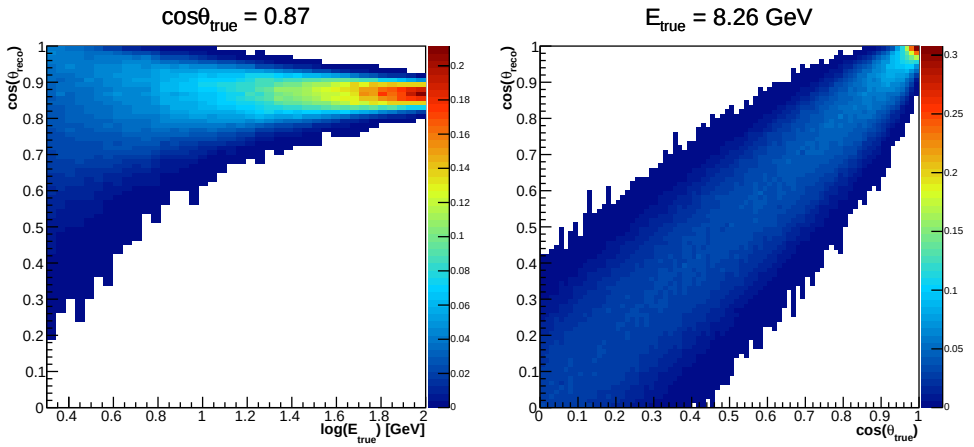

Figure 5.5: Energy dependency for θ_{reco} with no modifications (paramNMH with default values) for $\cos\theta_{true} = 0.87$ (left). The angular resolution gets better for higher energy (less spread and higher probability to reconstruct the true energy) (right) θ_{reco} is shown as function of θ_{true} for a fixed energy $E = 8.26GeV$. θ_{reco} gets better for angles close to the zenith (in the detector from below)

These two unmodified resolutions lead to the unmodified sensitivity plots Figure 5.6 and Figure 5.7 which will be used later as reference on the effect of the better resolution. A dependency on the mixing angle θ_{23} is apparent[3].
The sensitivity is given as confidential intervall to exclude the WH within 3 years. While the sensitivity for the IH stays below 3σ, the sensitivity of the NH even gets better than 4σ for $\theta_{23} > 47°$ To determine which channel (track/shower) is more important for sensitivity for each neutrino mass hierachy, the single sensitivity for track and shower is plotted for the NH (see Figure 5.6) and for the IH (see Figure 5.7). The total sensitivity is calculated through:

$$\sigma_{total} = \sqrt{\sigma^2_{track} + \sigma^2_{shower}}. \tag{25}$$

σ_total is the, in section 5 mentioned, square root of the χ^2-minimum. For further mentions the sensitivity is always given within 3 years. It can be seen from Figure 5.6, that the shower part (red line) is more important for sensitivity than the track part (blue line), especially for bigger θ_{23}. In Figure 5.7 the total sensitivity is lower than for NH, but the shower channel is still more important than the track reconstruction.

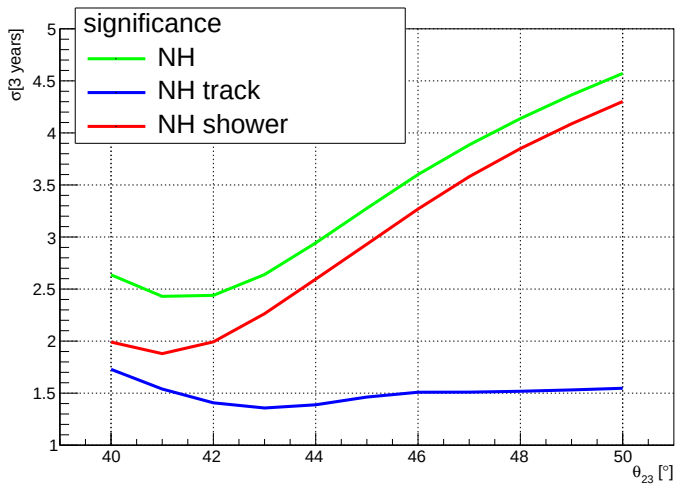

Figure 5.6: Sensitivity for the NH with the track channel (blue line) and the shower channel (red line) of the total sensitivity (green line) for variated θ_{23}. The sensitivity gets better for θ_{23} near 50°. This feature is shared for the shower channel but not the track channel.

5.2 Energy resolution

The energy resolution describes how well the energy of the neutrino can be determined through the Cherenkov signal of the secondary particle. The relativ energy error is dependent on the true energy of the neutrino. The relative error gets smaller for higher energies (see Figure 5.1). The energy resolution is better for

[3]the actual mixing angle θ_{23} is still unknown, but between 40° and 50°

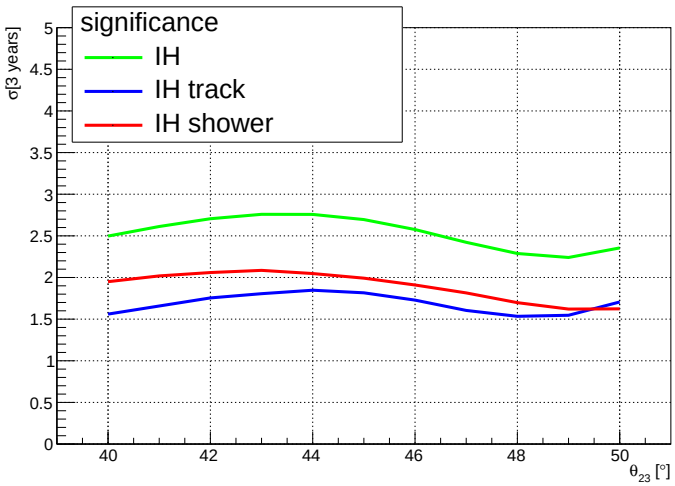

Figure 5.7: Plotted sensitivity for the IH with the track proportion (blue line) and the shower proportion (red line) of the total sensitivity for variated θ_{23}. The sensitivity is about independent of θ_{23}. The shower sensitivity is more important than the track sensitivity . Both proportions of sensitivity show the same independency of θ_{23}.

$\bar{\nu}$ CC events, because the inelasticity y is smaller for those events. The energy resolution is also better for $\overset{(-)}{\nu}_e$ CC (see Figure 5.8), because the determination is easier (determination by light yield of electromagnetic shower) in comparison to $\overset{(-)}{\nu}_\mu$ (determination by μ track length). To parameterize the energy resolution Figure 5.1 was fitted.
As a fit function Equation 26 was used, where a,b,c are fit parameters (see Tab. 5.3).

$$\frac{\Delta E}{E} = a + \frac{b}{E_\nu} + \frac{c}{\sqrt{E_\nu}}. \tag{26}$$

This parameterization was then implemented in the simulation to get an energy

	a	b	c
ν_e	0.0641	0.0214	0.3483
$\bar{\nu}_e$	0.0548	0.1436	0.2132
ν_μ	0.0804	0.0584	0.2698
$\bar{\nu}_\mu$	0.0935	0.2618	0.0324

Table 5.2: fit parameter for the different flavours with the fitfunction 26

resolution from the intrinsic limit [2]. This was done by replacing the Gaussian sigma, that was already in paramNMH, with the parameterization of the intrinsic limit. This ensures that the E_ν^{reco} has energy smearing (Gaussian) with the intrinsic limit as sigma. In Figure 5.8 and Figure 5.9 it can be seen that the distribution in energy resolution, especially for high energies, is narrower in comparison to

Figure 5.3 and Figure 5.4, where the Letter of Intent parameterization is inclosed. Additionally the maximum (mean energy see section 5.4)of the resolution plot is higher and due to that more certain. The energy determination for ν_e CC and especially for $\bar{\nu}_e$ CC is slightly better than for ν_μ CC and $\bar{\nu}_\mu$ CC. The energy resolution is narrower for $\overset{(-)}{\nu}_e$. This leads to the presumption that not only the resolution in general got better (more precise), but that especially track-like events can be resolved much better.

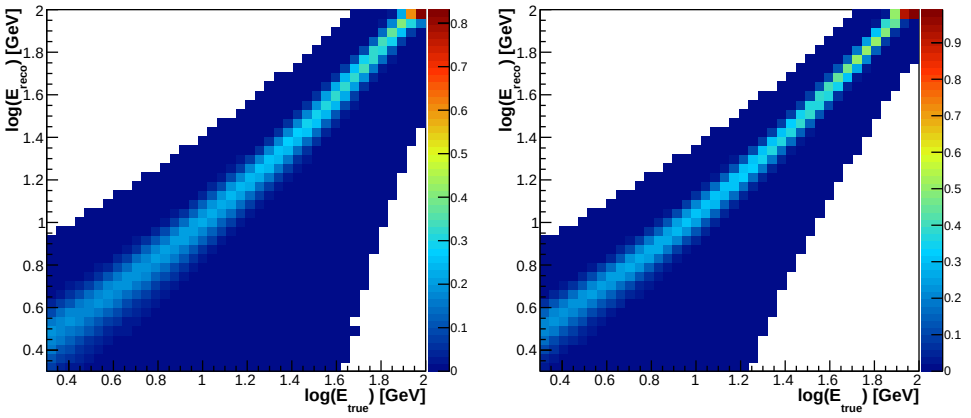

Figure 5.8: E_{reco} over true energy vor ν_e CC (left) and $\bar{\nu}_e$ CC (right) with the intrinsic limit as energy resolution

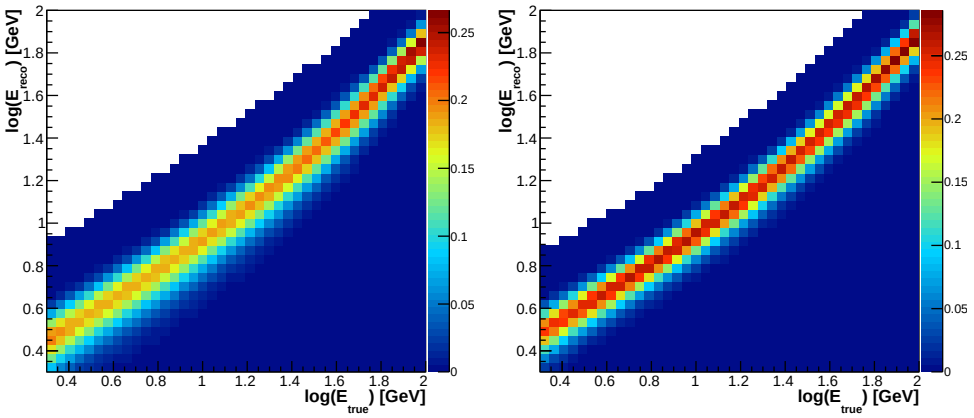

Figure 5.9: E_{reco} over true energy vor ν_μ CC (left) and $\bar{\nu}_\mu$ CC (right) with intrinsic limit energy resolution

After the better resolution was implemented, the sensitivity was investigated again (see Figure 5.10). To get a better understanding on how much influence the energy resolution has on the sensitivity a mid case resolution was added. This resolution is halfway between the instrinsic limit resolution and original resolution (Letter of Intent). As expected the intrinsic limit energy resolution sensitivity is the highest and the features like the θ_{23} dependency are still the same. The functions for sensitivity look similar for each energy resolution approach with just an offset for

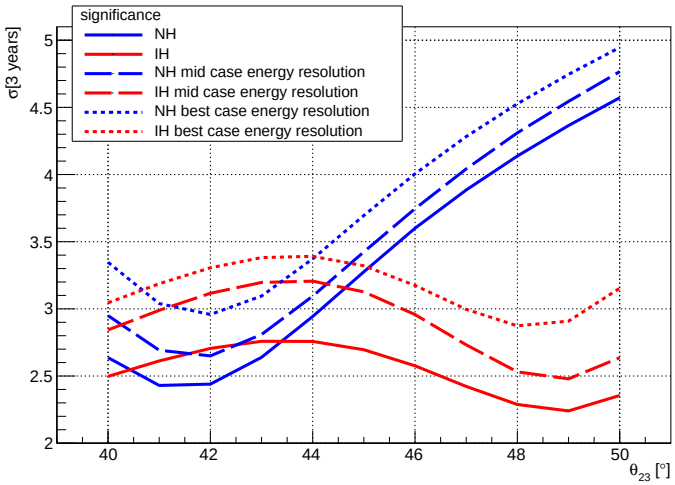

Figure 5.10: Comparison between the sensitivity with no modifications (solid lines), mid case (dashed lines) and the intrinsic limit energy resolution (dotted lines) for the NH (blue lines) as TH and IH (red lines) as TH

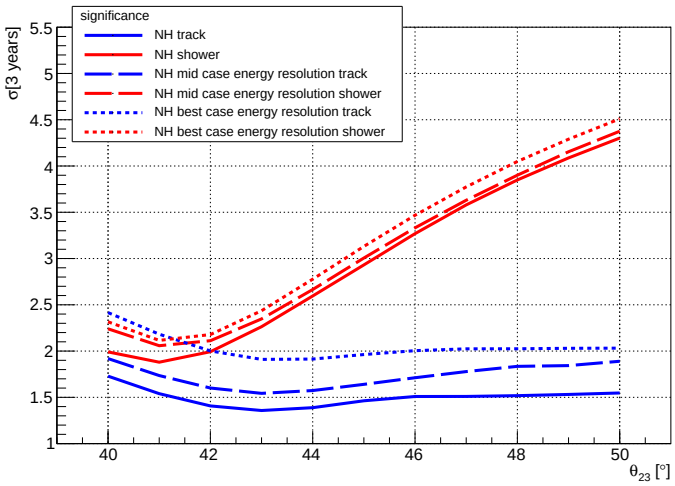

Figure 5.11: Comparison between the sensitivity with no modifications (solid lines), mid case (dashed lines) and the intrinsic limit energy resolution (dotted lines) for tracks (blue lines) and showers (red lines) assuming the NH as TH

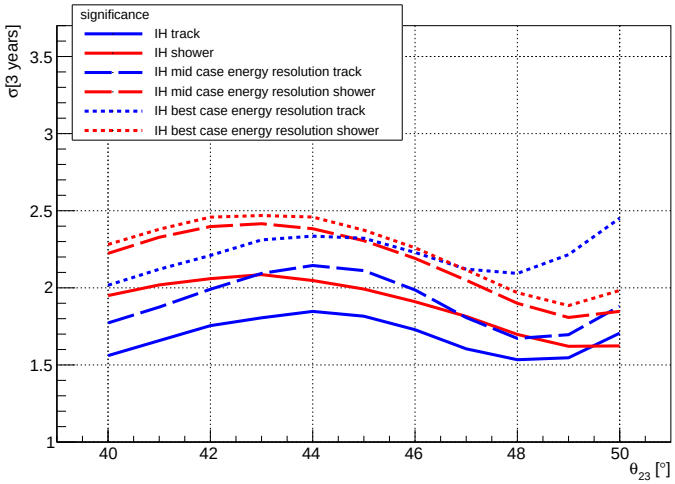

Figure 5.12: Comparison between the sensitivity with no modifications (solid lines), mid case (dashed lines) and the intrinsic limit energy resolution (dotted lines) for tracks (blue lines) and showers (red lines) assuming the IH as TH

better resolution. This offset is about 1σ for sensitivity with the energy resolution of no modifications and the one with the intrinisc limit energy resolution.
Figure 5.11 shows the contribution of track and shower channel to the sensitivity for the NH with different energy resolutions. The sensitivity as function of θ_{23} shows the same behaviour like the original implementation.
It can be noticed that improvement for track-like events is greater than that for showers, which comfirms the suggestion[4] that the track portion for sensitivivity can be improved a lot. A similar pattern can be noticed for the IH (see Figure 5.12). There is not much of dependency on θ_{23} in comparison to the original simulation, but an offset of about 0.5σ can be noticed.

5.3 Angular resolution

The density profile of Earth (see Figure 3.2) a neutrino has experienced depends on the angle on which the neutrino is detected in the detector. As mentioned in section 3.2 the density of matter in way propagation of the neutrino influences the neutrino oscillation. Another angular dependent effect on the oscillation is that neutrinos have different distances in which they traverse Earth for different angles. Both effects can cause errors and uncertainties, if the angle cannot be measured precise.
Like for energy there is also an intrinsic limit on the angular resolution. Figure 5.2 reveals that the angular resolution gets better for higher energies and like in section 5.2 for the energy resolution the direction resolution is also better for $\bar{\nu}$ CC than for ν CC, because of the smaller inelasticity y. The instrinsic limit was converted from a median error to a Gaussian sigma and then parameterized

[4] the presumption from the energy resolution histograms for ν_e CC and ν_μ CC

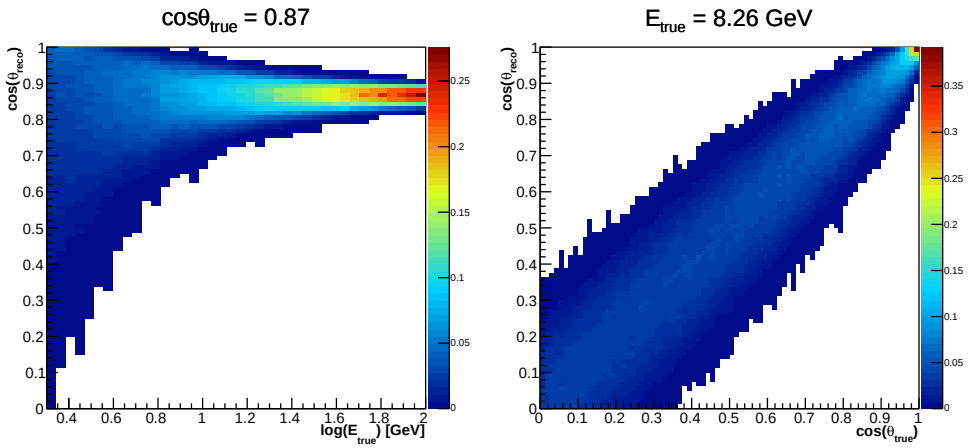

Figure 5.13: Energy dependency of $\cos(\theta_{reco})$ (left) for fixed $\cos(\theta_{true}) = 0.87$. The spread of the distribution gets smaller for higher energies with the center by $\cos(\theta_{reco}) = 0.87$. θ_{reco} as function of θ_{true} with fixed $E_{true} = 8.26GeV$ (right). The spread gets smaller for $\cos(\theta_{true}) \approx 1$ and the distribution describes an original straight line

(compare Figure 5.2 and [2]). The used fitfunction was

$$\Delta\theta = a + \frac{b}{E_\nu} + \frac{c}{E_\nu^2}. \tag{27}$$

	a	b	c
ν_e	$-4.94 \cdot 10^{-5}$	0.1164	0.4517
$\bar{\nu}_e$	-0.0007	0.0926	0.1398
ν_μ	0.0022	0.0700	0.6047
$\bar{\nu}_\mu$	0.0005	0.0621	0.2677

Table 5.3: Fit parameter for the different flavours with the fitfunction from Equation 27

The parameterization of the intrinsic limit was than implemented by replacing the old parameterization for the Gaussian sigma for the $\cos(\theta_{reco})$.
The sensitivity (see Figure 5.14) gets better for better angular resolution, but the effect is not so large compared to the energy resolution. This leads to the conclusion that the direction is not so important for sensitivity like the energy resolution. For the NH the improvement of sensitivity gets better for small θ_{23} where as for bigger θ_{23} the improvement is not as large.
Figure 5.15 and Figure 5.16 show the distinction between the track and shower channel in sensitivity.
Unlike for Figure 5.14 the sensitivity is not always better for the track channel with better angular resolution. For shower-like events the improvement in sensitivity NH is small, but has its maximum for small θ_{23}. The sensitivity for the track channel gets worse than the original for $\theta_{23} < 44°$

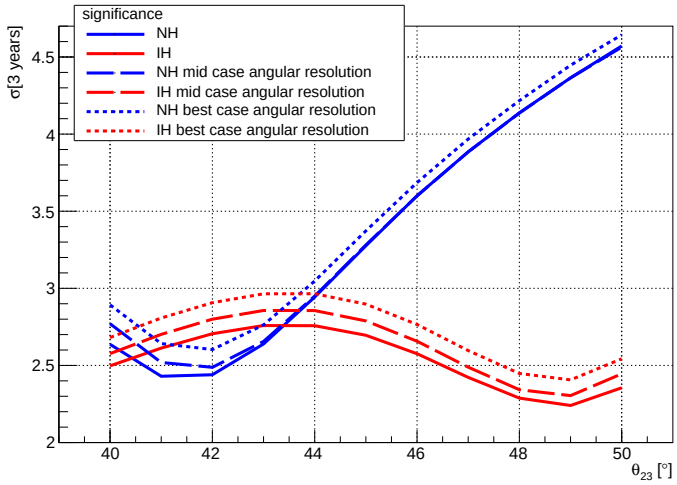

Figure 5.14: Comparison of the sensitivity for different angular resolutions. The lines with mid case resolution (dashed lines) and with the intrinsic limit resolution (dotted lines) show similar features and dependency on θ_{23} like the plot with no modifications.

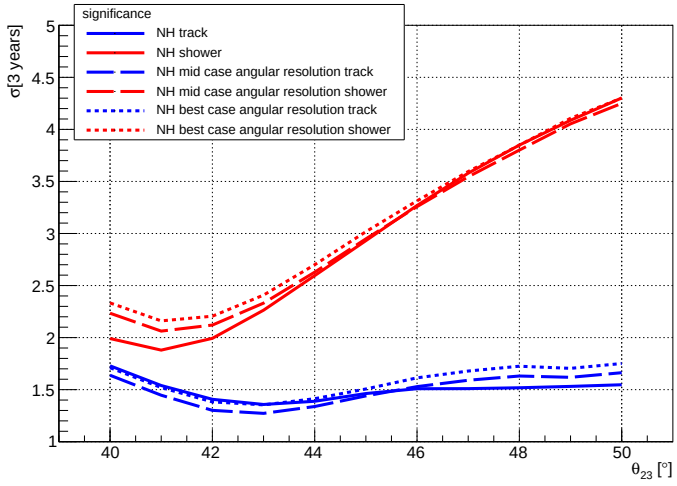

Figure 5.15: Comparison of sensitivity for the different angular resolutions for NH with a distinction between track (blue lines) and shower (red lines). For the track-like events the sensitivity is best for small θ_{23} with no modifications (solid lines) and worse for intrinsic limit resolution (dotted lines) and even worse for mid case resolution (dashed lines).

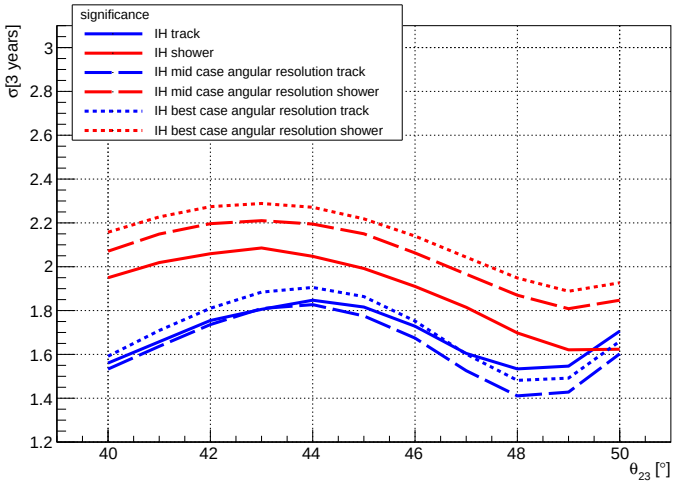

Figure 5.16: Comparison of sensitivity for the different angular resolutions for IH with a distinction between track (blue lines) and shower (red lines). For the shower channel the sensitivity of midcase resolution (dashed line) and intrinsic limit resolution (dotted line) is better than the original sensitivity (solid line).

For the track channel for the IH the intrinisc limit sensitivity is worse than the original for $\theta_{23} > 44°$.
Here we see that a better angular resolution does not imply a better sensitivity for each separate event channel (track/shower). At first this defies all intuition, but is explained easily by the fact that paramNMH makes a global fit of σ_{total} (see Equation 25). But that does not imply that this is a maximum for track/shower either. This hypothesis is supported by the fact that this effect is seen mostly for the track channel, because it does not contribute so much to the total sensitivity compared to the shower channel.

5.4 Mean energy

ν CC and $\bar{\nu}$ CC have different Cherenkov light yields. That means the Cherenkov light emitted for a certain energy is different. This is caused by the different inelasticities y of ν CC and $\bar{\nu}$ CC neutrinos.
The different light yield (see Figure 5.17) has to be considered for the sensitivity, especially for low energies[5]. For that case $\bar{\nu}$ CC produces more light in the detector than their ν CC counterpart. This causes an overestimated energy. To compensate this effect a modification, by parameterizing the light yield ratio, was added to paramNMH. For the parameterization

$$\text{light yield ratio} = 1 + a \cdot \left(\frac{E_\nu}{b}\right)^c \tag{28}$$

was used as fit function, with $a = 0.1112$, $b = 2.0520$, $c = -0.1431$. This was added by multiplying the parameterization of the light yield ratio (see Figure 5.17)

[5] $\sim 0GeV - 10GeV$

with the already in paramNMH existing parameterization for the mean energy. But this was only done for the mean energy of $\bar{\nu}$ CC, because the light yield ratio for ν CC to itself is constantly one.

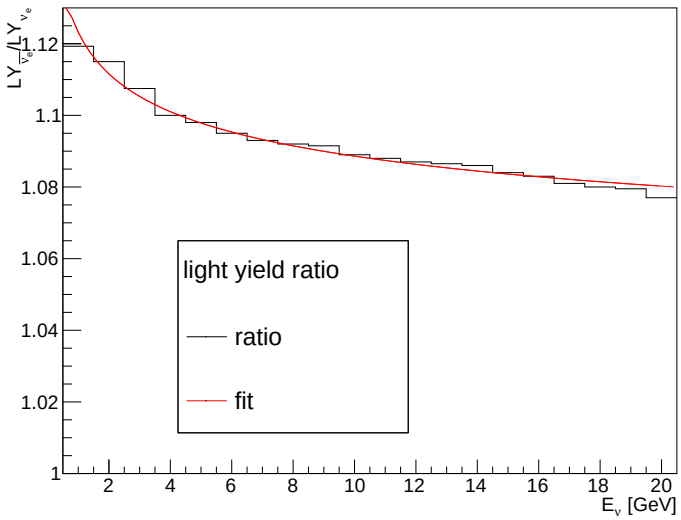

Figure 5.17: Parameterisation of the light yield ratio as function of the energy. The ratio (black line) was fitted with the function 28 (red line). [7]

The light yield ration starts with a bigger light yield (ratio of $\bar{\nu}/\nu \approx 1.12$) for $\bar{\nu}$ and than constantly decreases. An asymptotic approach to 1 is expected.
Figure A.1 and Figure A.2 show the energy resolution for ν_e CC,$\bar{\nu}_e$ CC, ν_μ CC and $\bar{\nu}_\mu$ CC. In comparison to Figure 5.3 and Figure 5.4 there are only changes for $\bar{\nu}$ notable. The energy resolution remains, as expected, the same, but the mean energy has shifted to higher E_{reco}. This is the expected overestimation.

The NH sensitivity (see Figure 5.18) for tracks increases the most. For shower the sensitivity gets better for $\theta_{23} < 46°$, but decreases constantly for bigger mixing angles. Until $\theta_{23} = 46°$, the sensitivity is better than with no modifications. Those two single sensitivities lead to a total sensitivity that is way better for small θ_{23} and then constantly decreases for increasing θ_{23}.
The IH sensitivity (see Figure 5.19) is improved relatively independent of θ_{23}. The improvement is slightly better for track than for shower.
In general the sensitivity increases but mostly due to the improvement of track sensitivity. The effect for the sensitivity with the modified mean energy is bigger than for the intrinsic limit direction resolution, but not as big as the effect of the intrinsic energy resolution.

5.5 Identical energy resolutions for $\overset{(-)}{\nu}_\mu$ and $\overset{(-)}{\nu}_e$

To test which effects the better energy resolution and mean energy for $\overset{(-)}{\nu}_e$ CC compared to $\overset{(-)}{\nu}_\mu$ CC has on the sensitivity, the energy resolution and mean energy of $\overset{(-)}{\nu}_\mu$ CC is replaced by the one of $\overset{(-)}{\nu}_e$ CC. This leads to Figure **??**, which shows

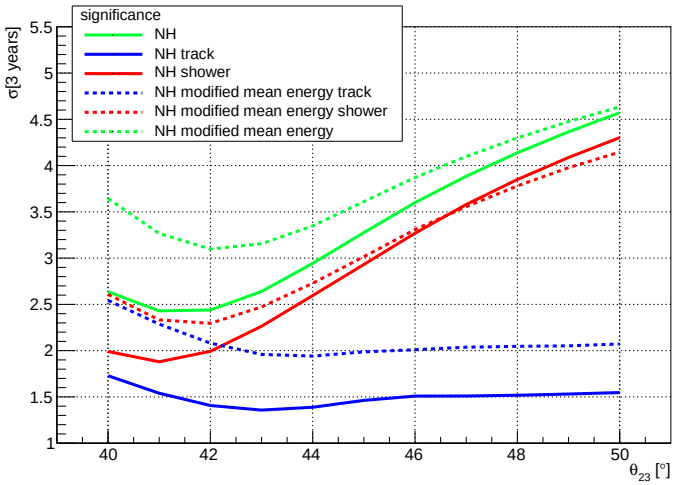

Figure 5.18: Comparison of the sensitivity for NH without (solid lines) and with modified mean energy (dotted lines). To compare the different event possibilities the sensitivity was plotted for total (green lines), for track (red lines) and shower (blue lines).

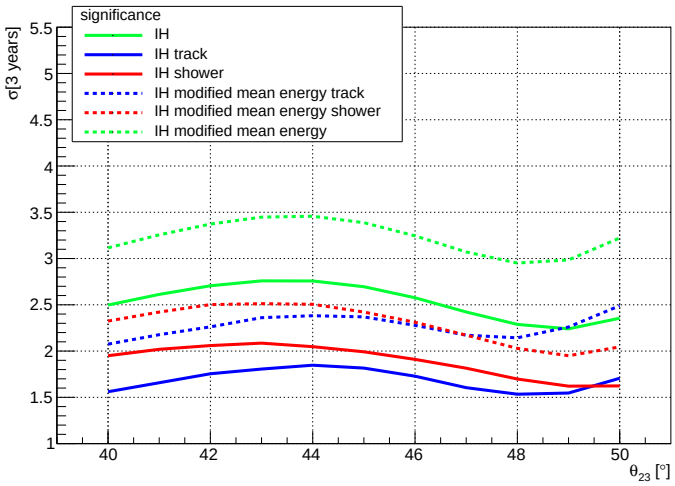

Figure 5.19: Comparison of the sensitivity for IH without (solid lines) and with modified mean energy (dotted lines). To compare the different event possibilities the sensitivity was plotted for total (green lines), for track (red lines) and shower (blue lines).

how good the energy gets reconstructed and as expected the energy resolution plot is identical to Figure 5.3. That is the case because the same parameterization is used in paramNMH for $\overset{(-)}{\nu}_e$.

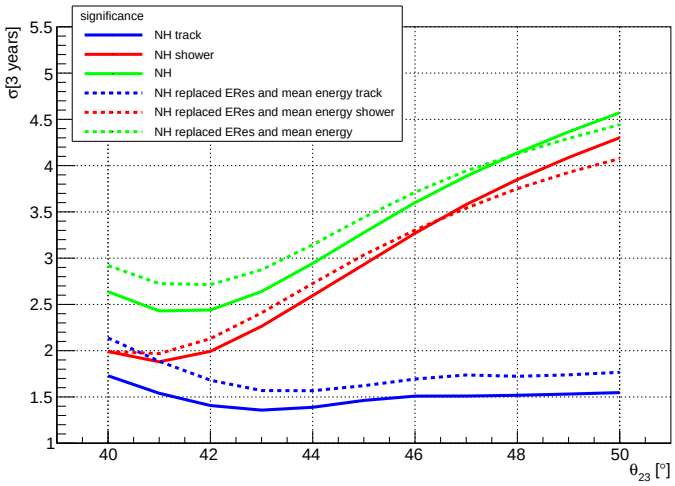

Figure 5.20: Sensitivity for NH with replaced $\overset{(-)}{\nu}_\mu$ CC energy resolution and mean energy (dotted lines) in comparison to the simulation with default parameters with a distinction between track (blue lines) and shower (red lines) and the total sensitivity (green lines).

Figure 5.20 shows only slight improvements to the original sensitivity and gets even worse than the original for $\theta_{23} > 48°$. This is caused by a deterioration in shower sensitivity all while the sensitivity for tracks gets better.

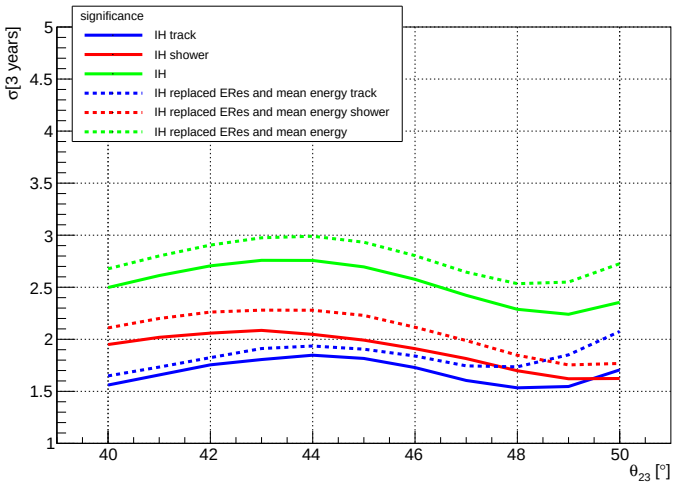

Figure 5.21: Sensitivity for IH with replaced $\overset{(-)}{\nu}_\mu$ CC energy resolution and mean energy (dotted lines) in comparison to the simulation with default parameters (solid lines) with a distinction between track (blue lines) and shower (red lines) and the total sensitivity (green lines).

Figure 5.21 shows the same modification only for the IH as TH. A small but

almost constant enhancement can be seen for the total sensitivity as well as the shower portion of sensitivity. The track channel shows a slight dependency on θ_{23} and gets better with bigger θ_{23}. The total improvement is about 0.3σ.
The replacing of the energy resolution with the the default parameter of paramNMH of $\bar{\nu}_e$ only makes a small impact on the total sensitivity and gets even worse than the original for big θ_{23}.

5.6 Particle identification

The particle identification is the classification of an event as track or shower. Ideally an event classified as track should be a ν_μ or a $\bar{\nu}_\mu$ interaction and an event classified as shower should be a NC interaction or CC for the other flavours, but in reality this strict distinction is not possible. Events can be classified wrongly as seen in Figure 5.22. This wrong identification occurs especially for low neutrino energies. Because in this energy regime the mean free path for μ is short and creates a similar Cherenkov light pattern in the detector to a shower-like interaction. The right identification is important, because it is the only way to determine which flavour composition of atmospheric neutrinos traversing Earth is detected.That is needed to compare it to the original composition to determine the oscillation probability.

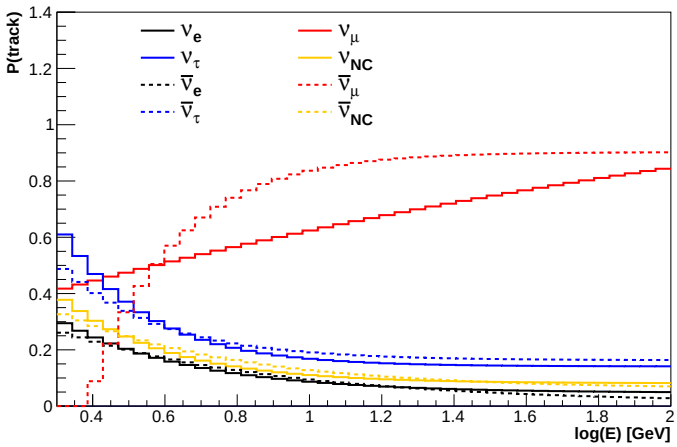

Figure 5.22: Probability to identify an event as track for ν_e CC (black solid line), $\bar{\nu}_e$ CC (black dashed line), ν_μ CC (red solid line), $\bar{\nu}_\mu$ CC (red dashed line), ν_τ CC (blue solid line), $\bar{\nu}_\tau$ CC (blue dashed line), ν NC (yellow line) and $\bar{\nu}$ NC (yellow dashed line) with default settings in paramNMH.

Figure 5.22 shows the probability to identify an event as track and it can be seen that the probability to classify an event wrongly as track goes up to 60% for ν_e CC for low energies. That leads to the conclusion that it is more likely for a ν_e CC to be classified as track than for a ν_μ CC in that energy regime (below $1.6GeV$). For high energies however the wrong classification for ν_e CC drops to around 20% and the right classification of ν_μ CC as track increases up to about 80%.

To see what influence the PID has for sensitivity the probability of events being identified as tracks was altered.
The probability of $\overset{(-)}{\nu}_\mu$ CC being classified correctly was increased with

$$P_{track,new} = P_{track,old} + \frac{1 - P_{track,old}}{a}. \tag{29}$$

Following alterations were carried out:

- a=4 : the probability was increased by a quarter of the distance to the perfect identification
- a=2 : the probability was increased by a half of the distance to the perfect identification
- a=1 : the probability was increased to the perfect identification (the probability is always 1)

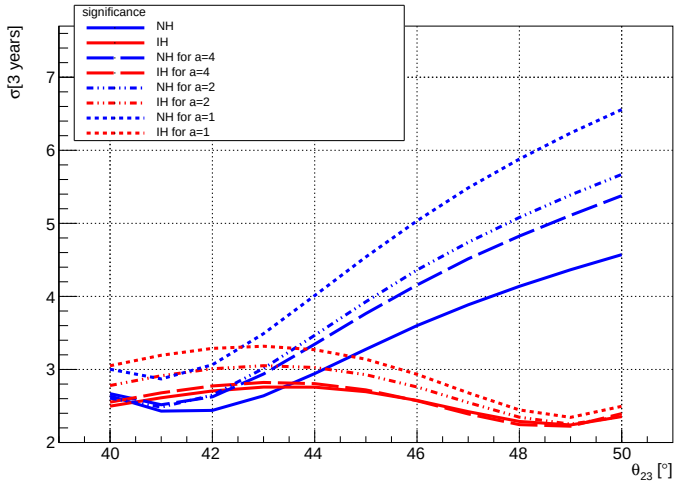

Figure 5.23: Comparison of sensitivity for NH (blue lines) and IH (red lines) as TH with different variations of, with Equation 29, modified PID.
No modifications → solid lines; a=4 → dashed lines; a=2 → dotted and dashed lines; a=1 → dotted lines

As expected the sensitivity increases if the PID is improved. The more the probability of a track-like event being identified as track increases the more the sensitivity increases. In Figure 5.23 it can be seen clearly that the improvement is larger for the NH than for the IH. Also notable is that the improvement for the NH gets greater for bigger θ_{23} where as for the IH it decreases.
Figure 5.24 shows the sensitivity for NH as TH with a distinction in track shower. The sensitivity improves for tracks, especially for bigger θ_{23}. Naively an improvement for shower is not be expcected, because only the probability of track identified as track was varieted, but this implies that less tracks are classified as shower and increase the sensitivity there.
For Figure 5.25 the improvement in the shower channel is not as large, but the

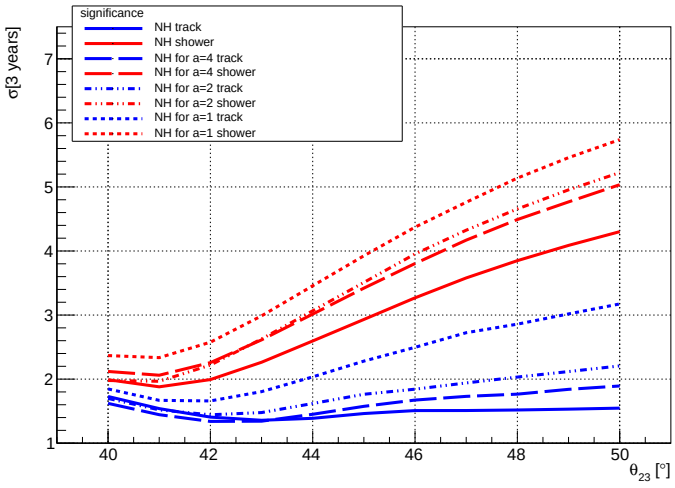

Figure 5.24: Comparison of sensitivity with NH as TH for track (blue lines) and shower (red lines) with different variations of, with Equation 29, modified PID. No modifications → solid lines; a=4 → dashed lines; a=2 → dotted and dashed lines; a=1 → dotted lines

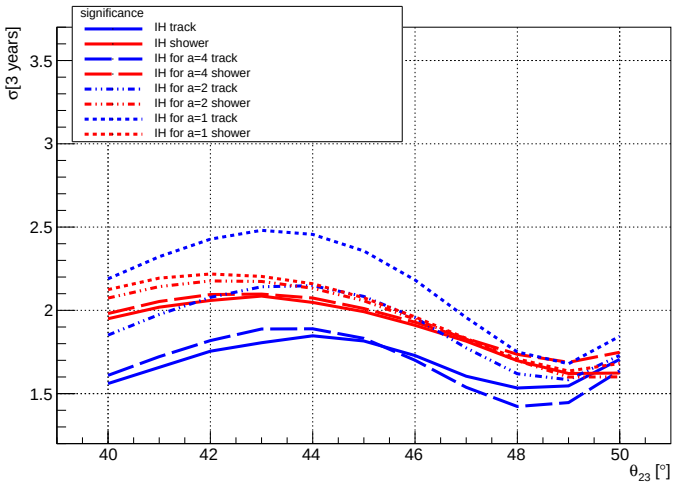

Figure 5.25: Comparison of sensitivity with IH as TH for track (blue lines) and shower (red lines) with different variations of, with Equation 29, modified PID. No modifications → solid lines; a=4 → dashed lines; a=2 → dotted and dashed lines; a=1 → dotted lines

track channel gets even better than the shower channel for the best case (a=1) for $\theta_{23} < 48°$. In combination the little improvement in the shower channel reduces the total improvement in sensitivity.
It is apparent that the improvement is larger for the NH than for the IH and both have inversed dependency in θ_{23} (for NH more improvement for bigger θ_{23} and for IH for smaller θ_{23}).
The second alteration was that the probability of true shower-like events being identified as tracks was decreased with

$$P_{track,new} = P_{track,old} - \frac{P_{track,old}}{b}. \tag{30}$$

With the following changes:

- b=4 : the probability was decreased by a quarter of the distance of not being classified as track
- b=2 : the probability was decreased by a half of the distance of not being classified as track
- b=1 : the probability was decreased to being never classified wrongly as track

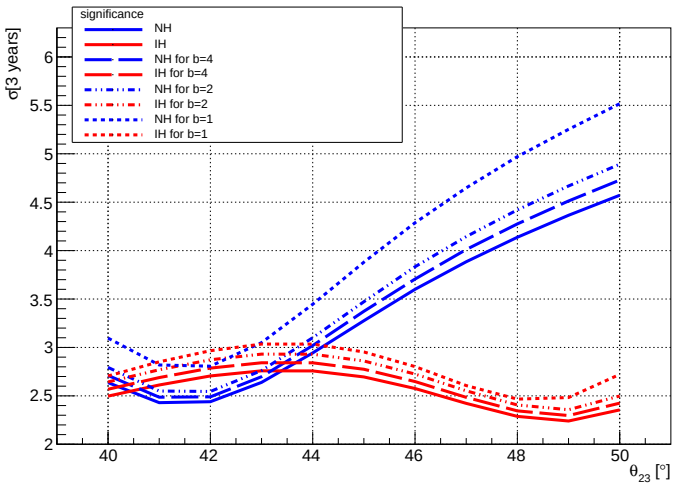

Figure 5.26: Comparison of sensitivity with NH (blue lines) and IH (red lines) with different variations of, with Equation 30 modified, PID.
No modifications → solid lines; b=4 → dashed lines; b=2 → dotted and dashed lines; b=1 → dotted lines

Figure 5.26 shows the sensitivity for NH and IH as TH with different PID modifications. The sensitivity for IH just shows an offset of maximal about $+0.25\sigma$ for the best case scenario of all true shower being identified as shower.
The sensitivity for NH shows greater betterment with up to about $+1\sigma$ for $\theta_{23} = 50°$. In general the improvement is less in comparison to the improvement in right classification (compare Figure 5.26 and Figure 5.23).

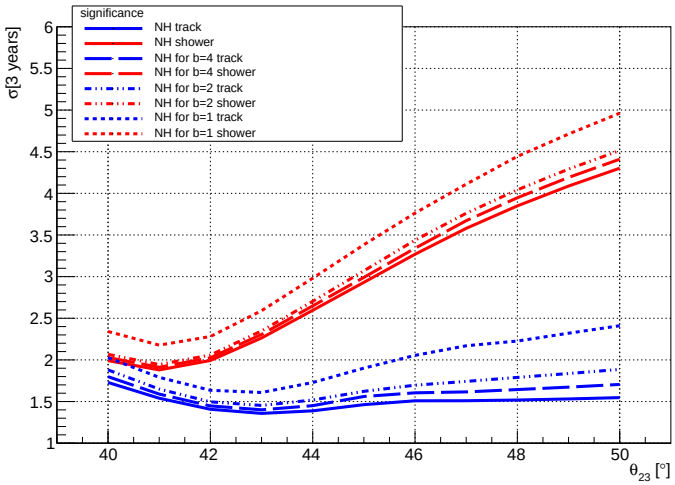

Figure 5.27: Comparison of sensitivity with NH as TH for track (blue lines) and shower (red lines) with different variations of, with Equation 30, modified PID. No modifications → solid lines; b=4 → dashed lines; b=2 → dotted and dashed lines; b=1 → dotted lines

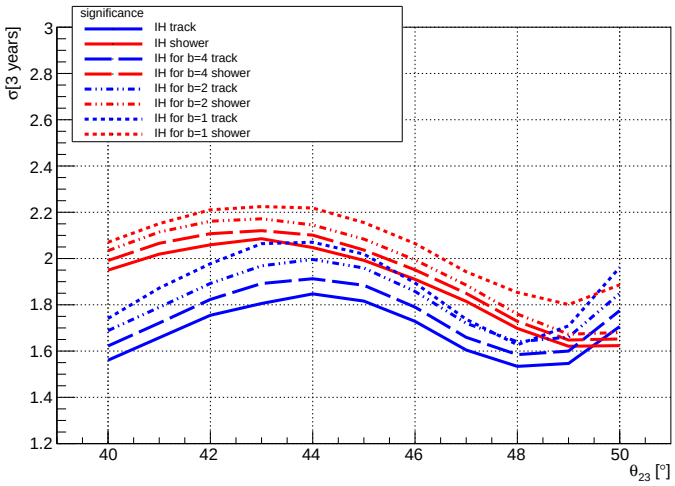

Figure 5.28: Comparison of sensitivity with IH as TH for track (blue lines) and shower (red lines) with different variations of, with Equation 30, modified PID. No modifications → solid lines; b=4 → dashed lines; b=2 → dotted and dashed lines; b=1 → dotted lines

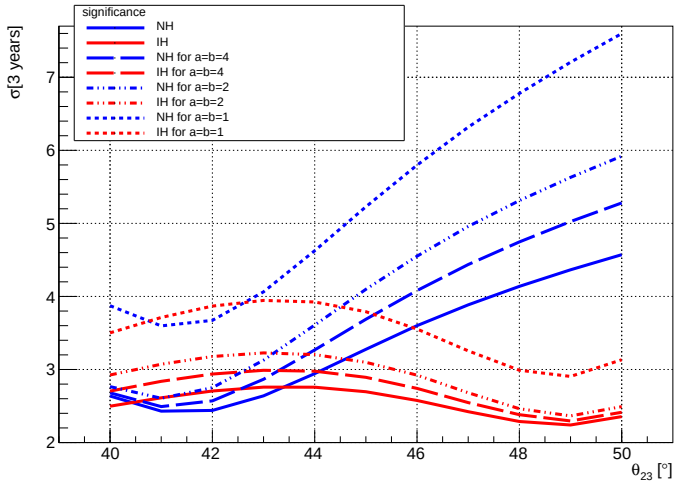

Figure 5.29: Comparison of sensitivity with NH (blue lines) and IH (red lines) with different variations of, with Equation 29 and Equation 30, modified PID.
No modifications → solid lines; a=b=4 → dashed lines; a=b=2 → dotted and dashed lines; a=b=1 → dotted lines

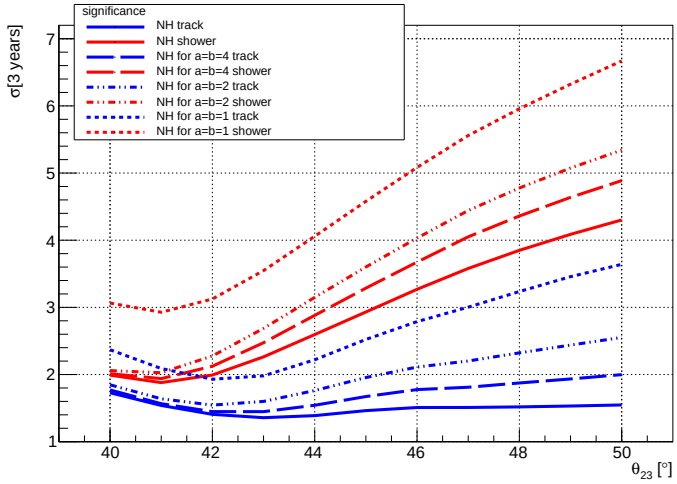

Figure 5.30: Comparison of sensitivity with NH as TH for track (blue lines) and shower (red lines) with different variations of, with Equation 29 and Equation 30, modified PID.
No modifications → solid lines; a=b=4 → dashed lines; a=b=2 → dotted and dashed lines; a=b=1 → dotted lines

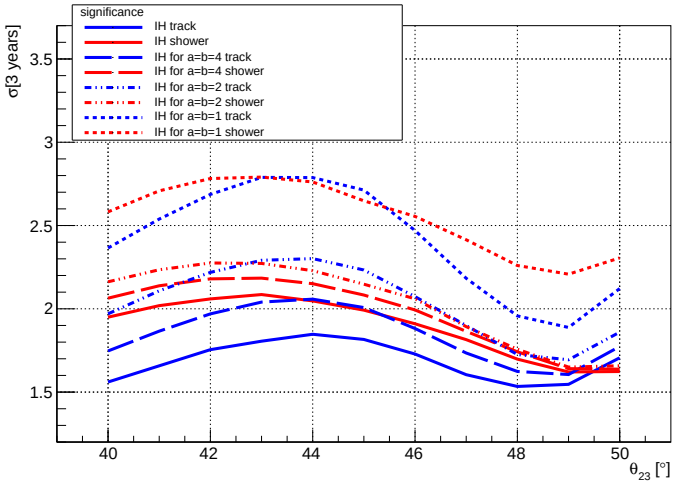

Figure 5.31: Comparison of sensitivity with IH as TH for track (blue lines) and shower (red lines) with different variations of with Equation 29 and Equation 30 modified PID.
No modifications → solid lines; a=b=4 → dashed lines; a=b=2 → dotted and dashed lines; a=b=1 → dotted lines

After that both modifications were implemented simultaneously.
Figure 5.29 shows the maximal potential of this modification. The sensitivity rises up to over 7σ for the best case scenario and for the smallest improvement of the PID over 5σ for NH[6]. The IH nearly reaches 4σ for best case and $\theta_{23} = 44°$. While the improvement for the IH gets worse for bigger θ_{23} the sensitivity for NH gets better.

The plot of sensitivity for NH in Figure 5.27 shows the differences between the sensitivity for track and for showers. It can be seen that the sensitivity gets better for larger θ_{23} and is for the best case about 0.8σ better for tracks and about 0.5σ for shower (for $\theta_{23} = 50°$).
The same was also done for the IH (see Figure 5.28). The betterment, which is a rather constant offset, is way less than for Figure 5.25 (only about 0.2σ).
The improvement for the track and shower portions of the sensitivity is very large (over 2σ for track and 1.5σ for shower $\theta_{23} = 50°$). This betterment gets less for smaller θ_{23} as well for the NH as the IH.
The improvement for the IH as TH in track and shower is not as great as for the NH (only about 0.5σ for shower and about 0.8σ for track). But in general the improvement for track is greater than for shower and gets less for bigger θ_{23}.
This show that the improvements in PID are especially in combination significant, when Equation 29 and Equation 30 are both implemented. Although a perfect assignment of the PID to the right event type is not possible even slight enhancements can improve the sensitivity significant.

[6] and $\theta_{23} = 50°$

5.7 Best case scenario

To get a look at what sensitivity could be achieved if all modifications[7] are implemented. paramNMH was modified to combine all those modifications. The combination of modified mean energy and intrinsic limit energy resolution leads to Figure B.1 and Figure B.2. Those two plots show the energy resolution for $\overset{(-)}{\nu}_e$ and $\overset{(-)}{\nu}_\mu$. As expected the plots show the features of both the modified mean energy (shift of the mean energy)[8] and of the intrisic limit energy resolution (smaller spread of energy distribution)[9].
The angular resolution is given by Figure 5.13, because no additional changes were made to this resolution [10].
This leads to the combined sensitivity described with Figure 5.32 and Figure 5.33. Figure 5.32 shows that the greatest improvements in sensitivity are for small θ_{23} (about 1σ) and that the improvements decline with increasing θ_{23}. It also shows that for θ_{23} the track channel has an improvement of about 1σ, but that decreases until the sensitivity for shower becomes lower than the original[11]. The track channel improves with a constant which is about 0.8σ.

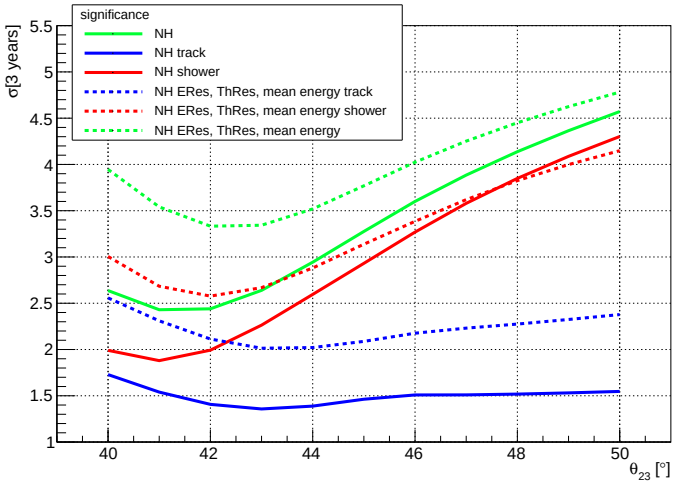

Figure 5.32: Comparison of sensitivity for NH with no modifications (solid lines) and with intrinsic energy, angular resolution as well as modified mean energy (dotted lines) with a distinction in track (blue lines), shower (red lines) and total sensitivity (green lines).

The sensitivity for IH is given by Figure 5.33. Here we can see an almost constant[12] gain in sensitivity (about 0.9σ on average). The improvement in track and shower is roughly the same (about 0.6σ).
This leads to the conclusion that the gain in sensitivity is slightly better for the

[7] see section 5.2, 5.3, 5.4 and 5.6
[8] compare with Figures A.1 and A.2
[9] compare with Figures 5.8 and 5.9
[10] only intrinsic direction resolution
[11] for $\theta_{23} = 48°$
[12] only little dependency on θ_{23}

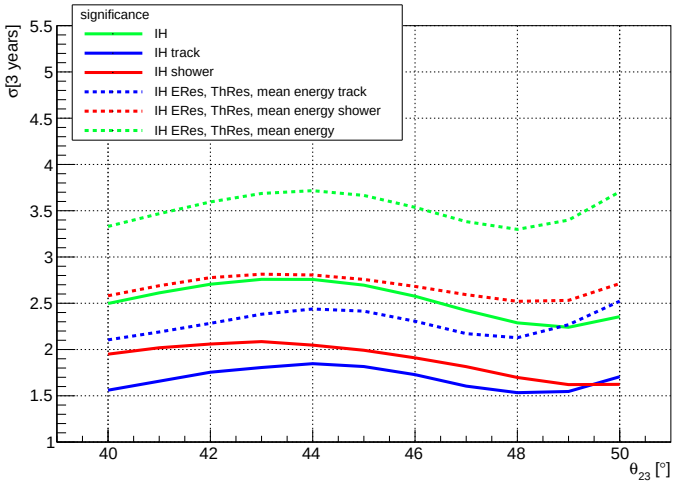

Figure 5.33: Comparison of sensitivity for IH with no modifications (solid lines) and with intrinsic energy, angular resolution as well as modified mean energy (dotted lines) with a distinction in track (blue lines), shower (red lines) and total sensitivity (green lines).

NH, but not significant.
After that combination of the modifications for angular and energy resolution as like as the modified mean energy another effect was added: the modified PID. In this case the PID which was modified with Equation 29 as well as Equation 30 was taken. As new reference for comparison the sensitivity with modified mean energy and intrinsic limit energy and angular resolution was taken (see Figure 5.32 and 5.33). Figure 5.34 shows the sensitivity with all hitherto made modifications. This shows as expected the greatest improvement with the sensitivity for NH getting over 8σ [13]. The IH gets a sensitivity with over 5σ in the best case [14]. The sensitivity for NH gets its biggest gain (about 3.5σ) for higher θ_{23}, while the IH has it biggest gain for $\theta_{23} = 44°$ the minimum is located for $\theta_{23} = 50°$.
Figure 5.35 shows the sensitivity for NH with a distinction for track and shower. The track portion of sensitivity makes a major improvement while the shower sensitivity only improves for bigger θ_{23} (improvement with up to about 2σ). For smaller mixing angles a decrease for shower sensitivity can be seen for the same reasons like in section 5.3. The track channel improves with about 2.8σ in its maximum ($\theta_{23} = 50°$) and about 1.2σ in its mimumum ($\theta_{23} = 40°$). While the improvements of track sensitivity for IH are smaller compared to NH, a huge advancement can be observed nevertheless. (1.7σ for $\theta_{23} = 44°$). The shower sensitivity on the other hand only improves marginally with less than 1σ in the maximum ($\theta_{23} = 42°$). For bigger mixing angles the sensitivity for shower gets even worse than the orignal.

In conclusion the already great improvement of modified mean energy and intrinsic limit energy and angular resolution can still be improved a lot with the modified

[13] for $\theta_{23} = 50°$ and the best case scenario for the PID
[14] for $\theta_{23} = [42°; 46°]$

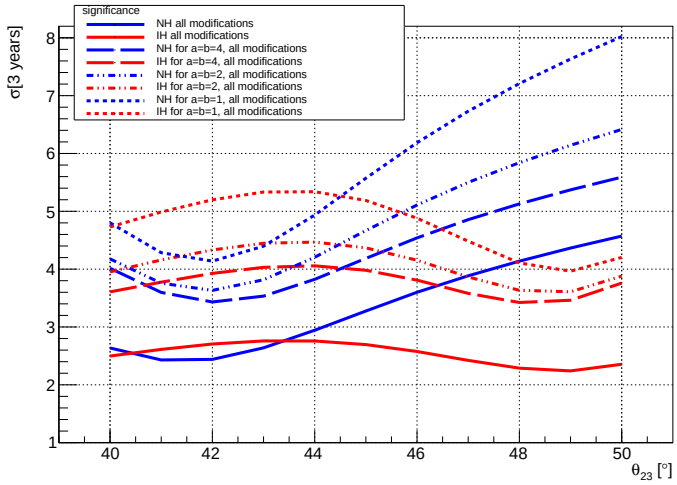

Figure 5.34: Comparison of the sensitivity for NH (blue lines) and IH (red lines) with modified mean energy, intrinsic limit angular and intrisic limit energy resolution with different variations of, with Equation 29 and Equation 30, modified PID.
no PID modifications → solid lines; a=b=4 → dashed lines; a=b=2 → dotted and dashed lines; a=b=1 → dotted lines

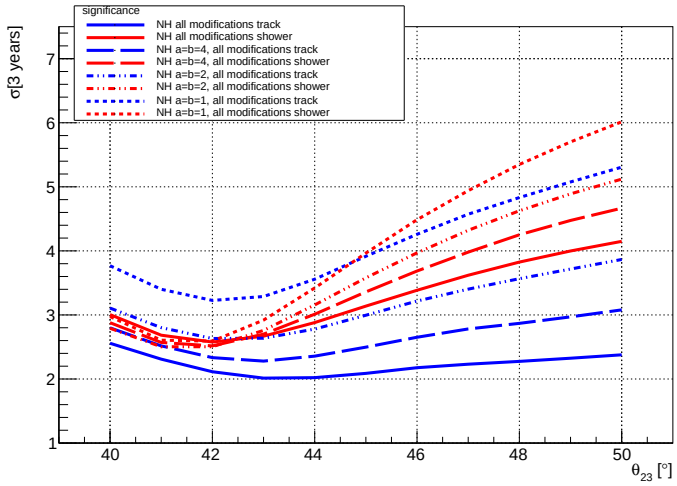

Figure 5.35: Comparison of the sensitivity for NH with a distinction in track (blue lines) and shower (red lines) with modified mean energy, intrinsic limit angular and intrisic limit energy resolution with different variations of, with Equation 29 and Equation 30, modified PID.
no PID modifications → solid lines; a=b=4 → dashed lines; a=b=2 → dotted and dashed lines; a=b=1 → dotted lines

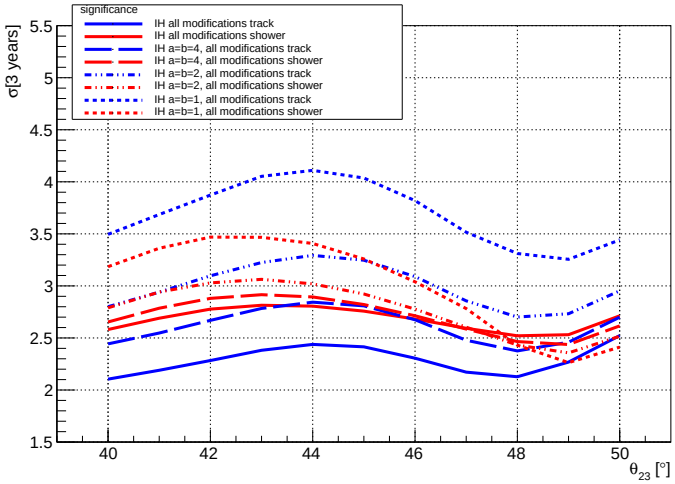

Figure 5.36: Comparison of the sensitivity for IH with a distinction in track (blue lines) and shower (red lines) with modified mean energy, intrinisc limit angular and intrisc limit energy resolution with different variations of, with Equation 29 and Equation 30, modified PID.
no PID modifications → solid lines; a=b=4 → dashed lines; a=b=2 → dotted and dashed lines; a=b=1 → dotted lines

PID, especially for the track portion of the NH sensitivity. The additional PID modification can get a total of improvement of sensitivity up to 3.5σ, which is enormous. The best case scenario with 8σ by $\theta_{23} = 50°$ would rule out the NH as TH with an uncertainty of $1.24 \cdot 10^{-13}\%$.

6 Conclusion and outlook

This thesis dealt with the potential of the KM3NeT/ORCA detector and how sensitive it is for the neutrino mass hierarchy with different assumptions for the detector response. paramNMH was used for the sensitivity studies as neutrino mass hierarchy sensitivity calculation code (see section 5). Although the best case modifications for PID and intrinsic limits resolutions are in reality not feasible, already small improvements in energy resolution (section 5.2) can cause a big gain in sensitivity. While the modified mean energy (section 5.4) and modified PID (section 5.6) have a not negligible effect on the sensitivity . Additionally it can be said for the PID that only a reducing of probability that a non track-like event is identified as track combined with the increasing of the probability in track-like events identified as tracks, causes a significant rise in sensitivity.
The improvement in angular resolution (section 5.3) contributes (even in the intrinsic limit) only little to the improvement in sensitivity. Also the effect on getting the same energy resolution for $\overline{\nu}_\mu$ like for $\overline{\nu}_e$ is rather small (section 5.5).
Another aspect of this thesis was the distinction between the sensitivity for NH and IH as TH: Here it can be said, that in general the NH detector is more sensitive towards the NH and also most of the time the improvement (e.g resolution) effects the sensitivity for NH more than for the IH, but the gain in sensitivity does not depend much on the mixing angle. That means that an improvement in reconstruction is likely to improve the sensitivity for the IH.
Another feature is that there is more room for improvement for track-like events. In almost any modification the improvement in the track channel is larger than the improvement in the shower channel.
In general a combined improvement for every mentioned modification can lead to a significant raise in certainty which neutrino mass hierachy is the one occuring in nature.

References

[1] Adrián-Martínez, S., Ageron, M., Aharonian, F., et al., Letter of Intent for KM3NeT 2.0. 2016

[2] Adrián-Martínez, S., Ageron, M., Aiello, S., et al., Intrinsic limits on resolutions in muon- and electron-neutrino charged-current events in the KM3NeT/ORCA detector. 2016

[3] Bellerive, A., Klein, J. R., McDonald, A. B., et al., The Sudbury Neutrino Observatory. 2016

[4] Eberl, T. 2018, Private communication

[5] Formaggio, J. A. & Zeller, G. P., From eV to EeV: Neutrino Cross Sections Across Energy Scales. 2013

[6] Giunti, C. & W.Kim, C. 2007, Fundamentals of Neutrino Physics and Astrophysics

[7] Hofestädt, J. 2017, doctoralthesis, Friedrich-Alexander-Universität Erlangen-Nürnberg (FAU)

[8] Honda, M., Athar, M. S., Kajita, T., Kasahara, K., & Midorikawa, S., Atmospheric neutrino flux calculation using the NRLMSISE00 atmospheric model. 2015

[9] JUNO. 2017, Neutrino mass hierachy, `http://www.staff.uni-mainz.de/wurmm/juno.html`

[10] Kajita, T., Atmospheric Neutrinos. 2004, New Journal of Physics

[11] Kajita, T., The Measurement of Neutrino Properties with Atmospheric Neutrinos. 2014, Annual Review of Nuclear and Particle Science, 64, 343

[12] Kamo, Y., Yajima, S., Higasida, Y., et al., Analytical calculations of four-neutrino oscillations in matter. 2002

[13] Katz, U. F., The ORCA Option for KM3NeT. 2016, Journal of Physics G: Nuclear and Particle Physics, 43(8), 084001

[14] Mikheev, S. P. & Smirnov, A. Y., Resonance amplification of oscillations in matter and spectroscopy of solar neutrinos. 1985, 42, 913

[15] Ohlsson, T. & Snellman, H., Three flavor neutrino oscillations in matter. 1999, J.Math.Phys. 41 (2000) 2768-2788; Erratum-ibid. 42 (2001) 2345

[16] Walter, C. W., The Super-Kamiokande Experiment. 2008

[17] Wolfenstein, L., Neutrino oscillations in matter. 1978, D 17, 2369

[18] Yañez, J. P. & Kouchner, A., Measurement of atmospheric neutrino oscillations with very large volume neutrino telescopes. 2015

[19] Zuber, K. 2012, Neutrino Physics

A Modified mean energy

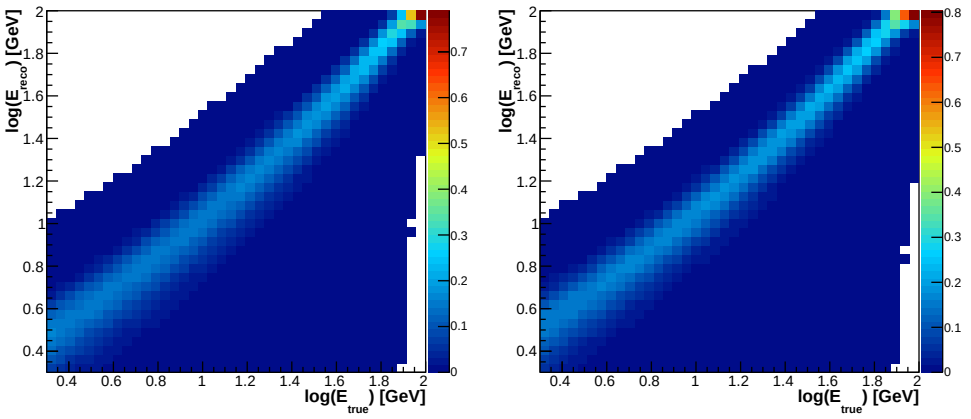

Figure A.1: E_{reco} over true energy with modified mean energy for ν_e (left) and $\bar{\nu}_e$ (right)

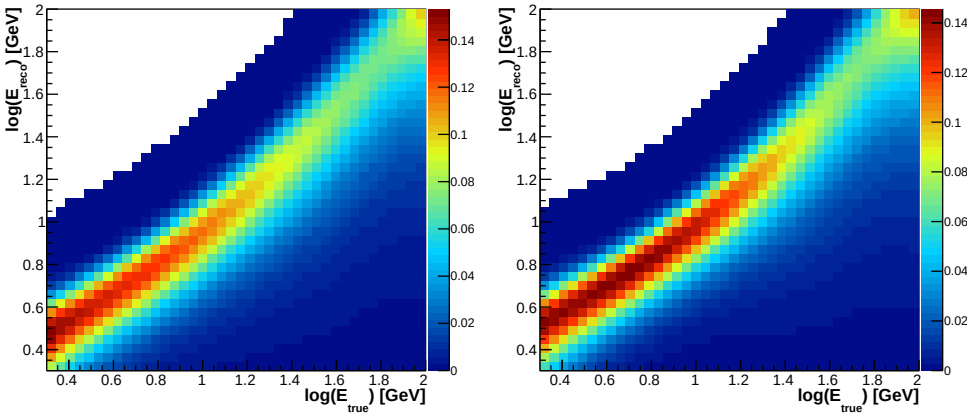

Figure A.2: E_{reco} over true energy with modified mean energy for ν_μ (left) and $\bar{\nu}_\mu$ (right)

B Modified energy resolution and mean energy

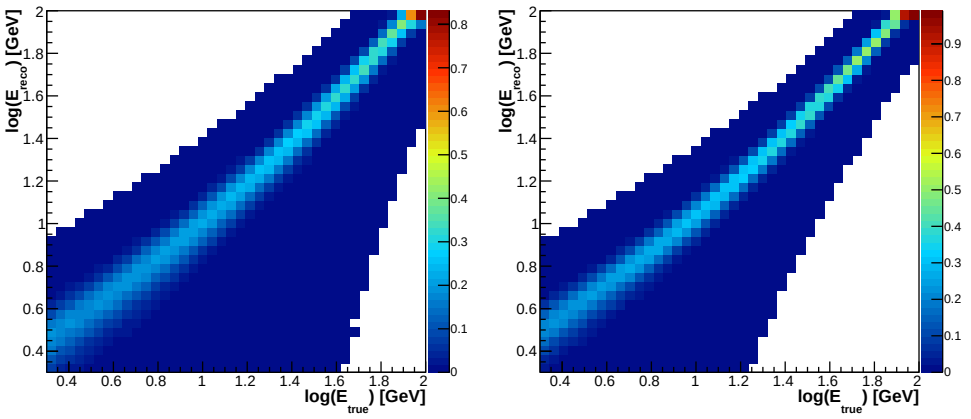

Figure B.1: E_{reco} over true energy with modified mean energy and intrinsic limit energy resolution for ν_e (left) and $\bar{\nu}_e$ (right)

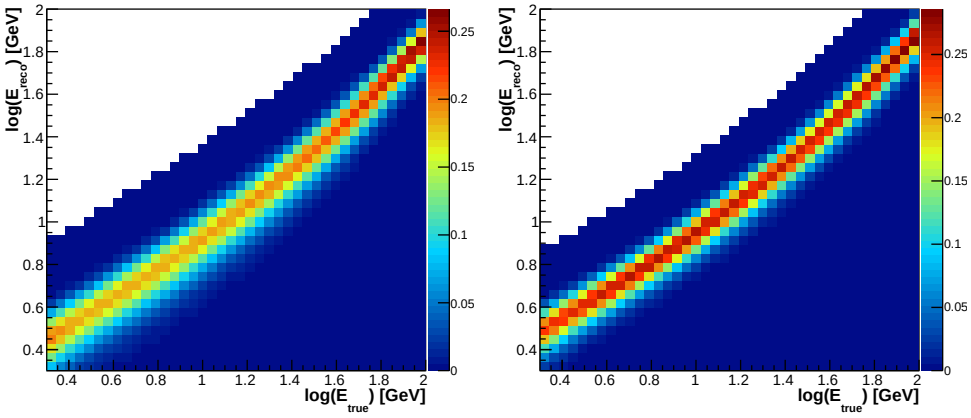

Figure B.2: E_{reco} over true energy with modified mean energy and intrinsic limit energy resolution for ν_μ (left) and $\bar{\nu}_\mu$ (right)

Statement of Authorship

I hereby certify that this thesis has been composed by me and is based on my own work, unless stated otherwise. No other person's work has been used without due acknowledgment in this thesis. All references and verbatim extracts have been quoted, and all sources of information, including graphs and data sets, have been specifically acknowledged.

Ort, Datum	Unterschrift

Acknowledgements

Hier möchte ich mich bei allen bedanken, die mich während der Erstellung dieser Bachelorarbeit untersützt haben. Ganz besonders möchte ich mich bedanken bei:

- Dr. Thomas Eberl und Dr. Jannik Hofestädt für die Vergabe eines so interessanten Themas und für zahlreiche und hilfreiche Vorschläge/Ideen.
- Marc Bruchner für die ständige Bereitschaft mir bei porgrammiertechnischen Problemen zu helfen und die Organisation des Tippspiels.
- Johann Brand, Daniel Runze und Benjamin Schwab für die produktive, lustige und hilfsbereite Atmosphäre im Büro
- Hans Konrad, Heike Konrad, Miriam Konrad und Alisa Helldörfer für die moralische und sprachliche Unterstützung bei meiner Arbeit